ELASTIC AND INELASTIC NEUTRON SCATTERING BY SILICON AND SULFUR

by

Gus A. Petitt

Department of Physics
Duke University

Date: _____

Approved:

_____
Harold W. Lewis, Supervisor

_____

_____

_____

_____

A dissertation submitted in partial fulfillment of the requirements for the degree of Doctor of Philosophy in the Department of Physics in the Graduate School of Arts and Sciences of Duke University

1964

L

ABSTRACT

The energy spectra of neutrons scattered by silicon and sulfur have been measured using time-of-flight techniques. Measurements were made at nine equally spaced scattering angles at incident neutron energies of 2.45, 2.85, 4.00, 4.90, and 5.80 MeV. In order to measure the variation with energy of the scattering cross sections, data were taken for more closely spaced energy intervals at a scattering angle of 60°. Elastic scattering and inelastic scattering to the first excited states of these nuclei were observed. The elastic scattering angular distributions are compared with the predictions of the optical model. The non-local potential of Perey and Buck with the potential well depths reduced slightly from their original values describes the shape elastic component of the scattering well for high incident neutron energies where fluctuation effects are small.

The inelastic scattering cross sections show large fluctuations which are ascribed to interferences between the amplitudes of the many excited levels in the compound system, although the angular distributions remain fairly isotropic. The inelastic scattering cross sections of silicon are compared to the predictions of the Hauser-Feshbach formula both with and without the Dresner "width fluctuation" correction. On the average, the magnitudes of these cross sections lie between the predictions of the corrected and uncorrected formulas. This suggests that in the ^{29}Si compound nucleus $\langle \Gamma^{J\pi} \rangle \approx D_{J\pi}$ rather than $\langle \Gamma^{J\pi} \rangle \gg D_{J\pi}$ which is necessary for the corrected formula to hold.

ACKNOWLEDGEMENTS

I wish to express my sincere appreciation to Dr. Philip R. Bevington for his guidance and encouragement during the course of this investigation. I should like to thank my co-workers Dr. S. G. Buccino, Dr. C. E. Hollandsworth, and Mr. C. Kapadia for their cooperation and assistance.

Appreciation is due Mr. S. Edwards and the entire nuclear physics group for their assistance with the accelerator. I wish to acknowledge the assistance given by Mr. Milt Whitfield and the staff of the instrument shop.

I wish to acknowledge the hospitality of the Department of Physics of Stanford University where most of this dissertation was written. Most of the computations involved in this research were carried out in the Stanford Computation Center.

Finally, I wish to thank Mrs. Shirley Stone for typing the manuscript.

G. A. P.

CONTENTS

LIST OF FIGURES

LIST OF TABLES

ELASTIC AND INELASTIC NEUTRON SCATTERING BY SILICON AND SULFUR

CHAPTER I

INTRODUCTION

This dissertation is concerned with the measurement of the angular distributions of neutrons which have been scattered after colliding with either silicon or sulfur nuclei. The neutrons may be either elastically scattered, leaving the target nucleus in its ground state, or they may be scattered inelastically, leaving the target nucleus in one of its excited states. The first few levels in silicon and sulfur are so widely spaced in energy that if a monoenergetic beam of neutrons is used to bombard these nuclei, time-of-flight techniques may be used to simultaneously detect and separately record the numbers of neutrons that are scattered elastically and those that are scattered inelastically at a particular scattering angle.

Predictions for the cross sections and angular distributions of the elastically scattered neutrons are obtained from the "optical model" of the nucleus. A computer code, ABACUS II (Auerbach, 1963) was used to make calculations of these angular distributions using three types of optical model potentials.

Predictions for the cross sections and angular distributions of inelastically scattered particles can be made under the conditions that the scattering takes place by formation and subsequent decay of a compound nucleus and that the "statistical model" correctly describes the compound system. The angular distributions are then given by the "Hauser-Feshbach"

formula (Hauser and Feshbach, 1952) or by certain modifications of this formula which depend on the assumed distribution of the partial widths of the energy levels in the compound nucleus. These formulas are also used to calculate the part of the elastic scattering angular distributions due to decay of the compound nucleus back to the ground state. These models and formulas are discussed in Chapter II.

The neutron time-of-flight method which was utilized to obtain the scattering data has proved to be a powerful tool in the field of neutron spectroscopy. The time-of-flight system used in the present work is described in Chapter III, which also includes details of associated equipment and the experimental procedure.

A brief discussion of the analytic procedure used to process the data is contained in Chapter IV. These results are compared with the theoretical predictions described above.

The final chapter summarizes the conclusions reached in the present work.

CHAPTER II

THEORY

A. Nuclear Reaction Mechanisms

Nuclear reactions may be conveniently classified in terms of the time scale in which they occur. At one end of the time scale are the "compound nucleus" reactions which occur in times on the order of 10^{-14} sec.; at the other end are the "direct reactions" which occur in times on the order of 10^{-23} sec. These two extreme cases can be understood by describing the general features of the interaction of the incident nucleon with the nucleus.

1. Compound Nucleus. One possible mechanism by which they may interact is for the incident nucleon to undergo a series of collisions with the nucleons in the nucleus, quickly spreading its excitation energy over the whole nucleus so that, after a certain relaxation time, statistical equilibrium is reached. The resulting nuclear state, which is a complex mixture of collective and single particle states, is said to be a state of the compound nucleus (Bohr, 1936). These states typically have very narrow widths ($\sim$ 10 keV) and consequently have long lifetimes.

The long lifetime of the compound nucleus is explained qualitatively as follows: The compound nucleus is composed of a superposition of many closely spaced levels. In such a case, the period P after which the initial

grouping of particles re-occurs, is very long. In particular, for the case of a state composed of a superposition of equidistant levels with spacing D this period is $\frac{2\pi\hbar}{D}$ (Blatt and Weisskopf, 1952). For typical average nuclear level spacings at the excitation corresponding to a few MeV incident neutron energy this period ($\sim 10^{-14}$ sec.) is many orders of magnitude larger than the period of a one-body motion in a potential well of nuclear size or the transit time of an incident particle through the nucleus ($\sim 10^{-23}$ sec.). Thus, sufficient energy for escape will be concentrated on one particle or cluster of particles very infrequently. Even when enough energy is concentrated on one particle for it to escape, there is only a finite probability, given by the transmission factor for penetrating the potential barrier, that the particle will actually escape.

In Bohr's original hypothesis, it was assumed that after statistical equilibrium is reached, the system loses all "memory" of its mode of formation. Thus, there is no correlation between the modes of formation and decay other than that required by the most elementary conservation laws such as those of energy and angular momentum. As a consequence, the decay of the compound nucleus is independent of its mode of formation.

2. Direct Reactions. The compound nucleus is not always formed when an incident nucleon penetrates the nucleus. Instead, the incident particle may interact with only one particle or cluster of particles in the nucleus. It may transfer most of its momentum and energy to this particle which then escapes in a so-called "knockout" reaction; or the incident nucleon may scatter inelastically by giving up part of its momentum to a single particle in the nucleus. These are examples of "direct reactions", so called because they take place in about the same time as the transit time of the incident

nucleon through the nucleus. Since the incident wave packet is not appreciably delayed in passing through the nucleus, the phases of the partial waves in the incident channel are correlated with the partial waves in the exit channel. Thus, for direct reactions, there will be strong interference effects which may result in strong forward or backward peaking of the angular distribution of the emitted particles.

As another consequence of their short lifetimes, the widths of levels which are excited by direct reactions are very wide, and the cross section as a function of energy does not exhibit the narrow resonances that are characteristic of compound nucleus reactions at low energies.

Despite the enormous difference in the time scale between direct and compound reactions, it is also plausible that reactions should be pictured as sequential processes in which the incident nucleon first interacts with one nucleon or perhaps several. Whether the reaction is direct or compound then depends on whether the energy of the incoming particle is subsequently shared with more nucleons, or whether this process ceases and a particle is emitted before equilibrium is reached.

This sequential picture also indicates that compound reactions might display some of the properties of direct reactions. Feshbach (1958) has postulated the existence of "doorway" states in the compound nucleus formation. These states would be formed as the first of many possible sequences of reactions leading from the entrance channel to the compound nucleus and would be characterized by a considerable similarity with the entrance channel state. Such a state, for example, might be a "two particle-one hole" state which would result when a bombarding particle excites one of the nucleons in the nucleus above the Fermi sea in a straightforward two-body interaction. Once this state is formed, it might immediately decay back into the entrance

channel (direct elastic scattering) or it might decay into a more complicated state of the compound system. This latter process could continue indefinitely until finally the compound nucleus would be formed.

The cross section for compound nucleus formation would be enhanced for incident particle energies corresponding to the excitation energy of the doorway state. This would give rise to large compound nucleus cross sections with broad resonances similar to direct reaction cross sections.

3. Statistical Model. At very low excitation energies in the compound nucleus, for example just above the threshold for neutron emission, the widths of the nuclear levels are very narrow (as narrow as a few eV), and their average spacing is large enough so that they are completely separated. If the compound nucleus is formed by the excitation of one of these levels, then the assumption that the formation and decay of the compound nucleus is completely independent is obviously valid. The Breit-Wigner formalism for describing the cross sections for the excitation of these levels has been extremely successful in describing many kinds of experimental data in this energy region. In this formalism, the cross section for the reaction leading from state a to state b is written

$$\sigma(a,b) = \sigma_c(a) \frac{\Gamma_b}{\Gamma}$$

where $\sigma_c(a)$ is the cross section for the formation of a compound nucleus by the particle a and $\frac{\Gamma_b}{\Gamma}$ is the probability that the particle b is emitted by the compound state. Thus, the formula for describing the reaction can be separated into two independent parts.

As the excitation energy increases, however, the level spacing rapidly decreases. Fig. 1 shows this roughly exponential decrease in spacing with

Figure 1. Number of Compound Nucleus Energy Levels vs. Excitation Energy

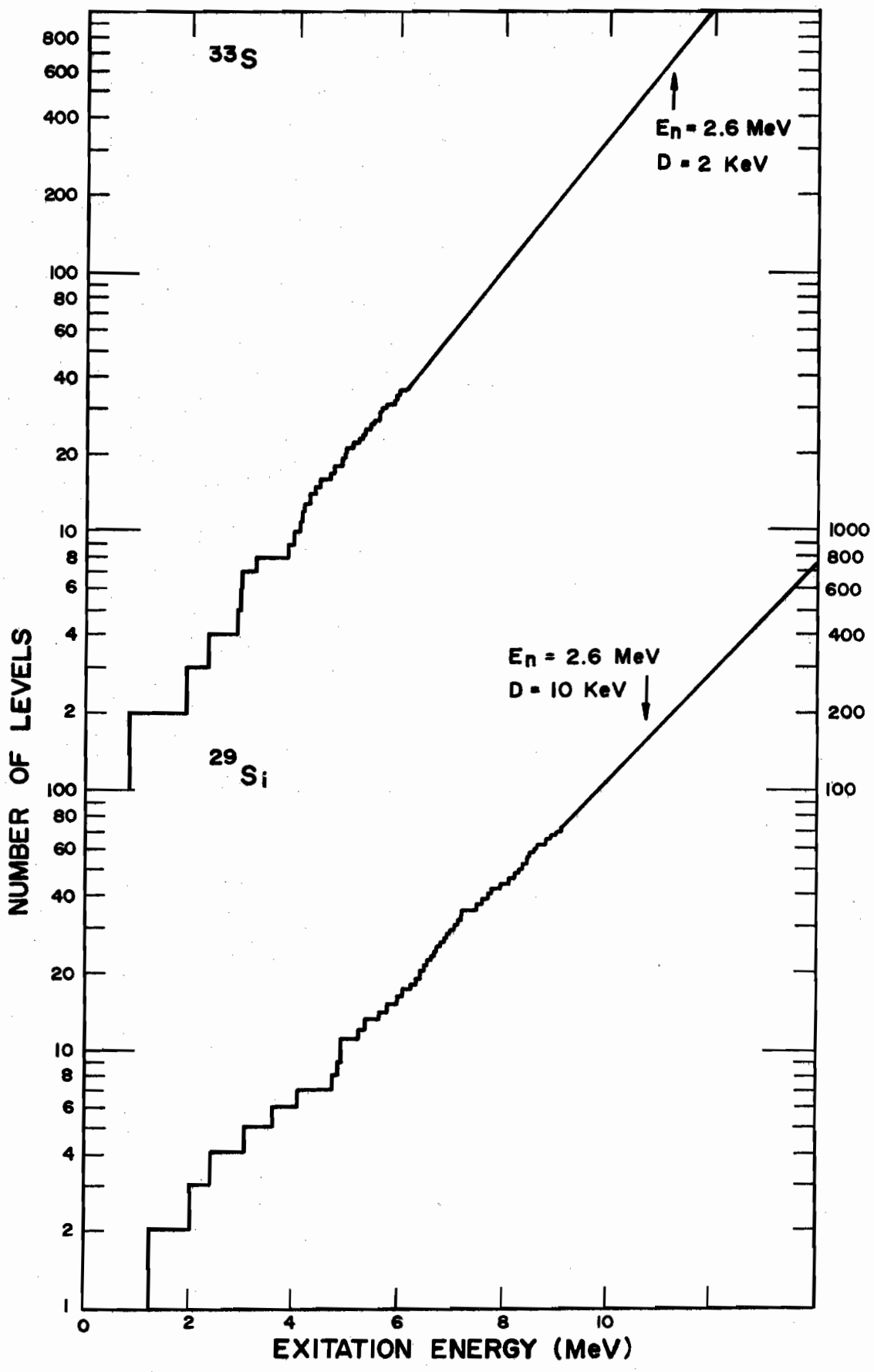
^{33}S
E_n = 2.6 MeV
D = 2 KeV
^{29}Si
E_n = 2.6 MeV
D = 10 KeV
NUMBER OF LEVELS
EXITATION ENERGY (MeV)
0
2
4
6
8
10
1
2
4
6
8
10
20
40
60
80
100
200
400
600
800
1000

excitation energy for silicon and sulfur. At the same time, the probability for emission of the incident particle increases, and many new decay channels open up. Their partial widths must be added to the total width, and the result is that the total width rapidly increases as the excitation energy increases. By the time the compound system has reached an excitation corresponding to about an MeV incident neutron energy, the compound nucleus levels have begun to overlap. When this occurs, there is no guarantee that the independence hypothesis holds. The reasons for this can be summarized as follows:

1) The independence hypothesis is based on the assumption that the compound state is so long lived that a state of statistical equilibrium is reached before the system decays. As the widths of the levels increase, however, the lifetime of the compound system, which is given ~~rougly~~ roughly by the relation $\tau = \hbar/\Gamma$, correspondingly decreases. Thus, as the energy increases, it becomes increasingly doubtful that equilibrium can be reached before the system decays.

2) The simple Breit-Wigner formalism no longer describes the reaction. The formula used to describe the reaction involves sums over products of pairs of scattering amplitudes for transitions from the various open channels to the compound system. There is no way of obtaining experimental information about the individual amplitudes; only average values can be calculated and compared with experiment and the values of these averages depend on the distribution of the amplitudes and the correlations between their sizes and phases.

In order to re-establish the independence hypothesis, the assumption is usually made that in the region where many levels overlap and the average total width is much larger than the average level spacing for a given angular momentum J and parity π ($\langle \Gamma^{J\pi} \rangle \gg D_{J\pi}$) the widths and phases of the partial

amplitudes involved in the calculations are randomly distributed and uncorrelated. Thus, when the contributions from many levels are summed, the cross terms will cancel, eliminating interference between different partial waves. Then, when the further assumption of random distribution of partial widths is invoked, it is again possible to separate the cross section into two parts, one corresponding to the formation of the compound nucleus and the other to its decay. This separation is possibly only if $\langle \Gamma^{J\pi} \rangle \gg D_{J\pi}$ at the excitation of the compound nucleus.

B. Elastic Scattering

1. Optical Model. Prior to about 1953, it was assumed that an incident nucleon after penetrating a nucleus immediately interacts with the individual nucleons in the nucleus through the strong, short-range nuclear force to form a compound nucleus. Predictions for neutron cross sections (Feshbach and Weisskopf, 1949) based on this assumption disagreed with experimental measurements of these quantities (Barschall, 1952). This and other disagreements between theory and experiment led to the introduction of a model (Feshbach, Porter, and Weisskopf, 1954) for describing the interaction of nucleons with nuclei which, because of its analogy to optics, is called the "optical" model or "cloudy crystal ball" model. This model describes the interaction in terms of a single complex potential

$$U = V + iW \tag{1}$$

In the first studies of this model, a simple square well potential was assumed

$$\begin{aligned} V &= V_0 \ , \quad W = W_0 \qquad r \leq R \\ V &= 0 \ , \quad W = 0 \qquad r > R \end{aligned} \tag{2}$$

Subsequently, more sophisticated well shapes have been used.

The basic assumption of the optical model is that, on the average, the complicated interactions of the incident nucleon with the nucleus may be approximated by a simple nucleon-potential interaction where the potential results from an average over all the individual nucleon interactions in the nucleus. This was suggested by the success of the shell model in describing nuclear properties. In the shell model of the nucleus, the individual nucleons are pictured as being in well defined quantum states, moving in an average central potential due to all the other nucleons. The interaction of an incident nucleon with the real part of the optical potential corresponds to a nucleon entering the shell model potential well without disturbing any of the nucleons in their ground state orbits. The incident nucleon will slightly perturb the shell model potential when it penetrates the nucleus so that the potential it sees will not be exactly the same as that seen by a nucleon in the ground state. However, this is presumably a very small effect (Perey and Buck, 1962).

In quantum mechanics, an imaginary potential represents a particle sink. Thus, the imaginary part of the optical potential describes the probability that an incident nucleon will be removed from the incident channel. In the optical model description, these particles disappear. Therefore, the model only describes the situation in the entrance channel.

This model cannot, of course, reproduce the fine resonance structure that is exhibited by neutron cross sections for low incident neutron energies. In this energy region, the model predicts only the behavior of the cross section averaged over an energy interval large compared to the spacing between resonances. The optical model cross sections are obtained by taking the average value of the actual cross sections over an energy range $\Delta\epsilon = I$ such that I contains many closely spaced resonances.

It is convenient to first separate the expressions for scattering and reaction cross sections into partial cross sections for each orbital angular momentum l which are usually expressed in terms of reflection factors, η_l , as follows:

$$\begin{aligned} \sigma_{el}^{l} &= \pi \lambda^2 (2l+1) |1-\eta_l|^2 \\ \sigma_{r}^{l} &= \pi \lambda^2 (2l+1)(1-|\eta_l|^2) \end{aligned} \tag{3}$$

the η_l , in turn, may be expressed in terms of complex phase shifts

$$\eta_l = \exp(2i\xi_l) \tag{4}$$

where

$$\begin{aligned} \xi_l &= \rho + i\phi \\ |\xi_l| &\leq 1 \end{aligned} \tag{5}$$

The optical model cross sections are

$$\begin{aligned} \bar{\sigma}_{el}^{l} &= \frac{1}{I}\int_{\epsilon - I/2}^{\epsilon + I/2} \sigma_{el}^{l}\, d\epsilon = \pi \lambda^2 (2l+1)\overline{|1-\eta_l|^2} \\ \bar{\sigma}_{r}^{l} &= \frac{1}{I}\int_{\epsilon - I/2}^{\epsilon + I/2} \sigma_{r}^{l}\, d\epsilon = \pi \lambda^2 (2l+1)(1-\overline{|\eta_l|^2}) \end{aligned} \tag{6}$$

We define the "shape elastic", "fluctuation", and "compound nucleus formation" cross sections respectively as

$$\begin{aligned} \bar{\sigma}_{se}^{l} &= \pi \lambda^2 (2l+1)|1-\bar{\eta}_l|^2 \\ \bar{\sigma}_{fl}^{l} &= \pi \lambda^2 (2l+1)\{\overline{|\eta_l|^2} - |\bar{\eta}_l|^2\} \end{aligned} \tag{7}$$

$$\begin{aligned} \bar{\sigma}_{c}^{l} &= \bar{\sigma}_{fl}^{l} + \bar{\sigma}_{r}^{l} = \pi \lambda^2 \{1-|\eta_l|^2\} \\ &= \pi \lambda^2 (2l+1)\, T_l \end{aligned}$$

where T_l is the transmission coefficient for formation of the compound state.

We assume that the average value of η_l over the energy range I is a smooth function of ϵ . Then $\bar{\sigma}_{se}^{l}$ and $\bar{\sigma}_{c}^{l}$ have the form of a scattering

and reaction cross section of a new and different scattering problem whose phase varies slowly with energy.

Analogously, the angular distributions for shape elastic scattering will be given by

$$\left(\frac{d\bar{\sigma}}{d\Omega}\right)_{se} = |\bar{f}|^2 \tag{8}$$

where $\bar{f}$ is an energy averaged scattering amplitude

$$\bar{f} = \frac{\lambda}{2i}(1-\bar{\eta}_\ell)P_\ell(\cos\theta) \tag{9}$$

The problem then is to solve Schroedinger's equation in the presence of a single-particle, complex potential, such that the resulting reflection factors η_ℓ have the correct values for the average factors $\bar{\eta}_\ell$ of the optical model cross sections.

Since $\bar{\sigma}_{fl}$ depends on $\overline{|\eta_\ell|}$ as well as $|\bar{\eta}_\ell|$, the optical model cannot predict values for this cross section. Its value is known in two limiting cases, however. At sufficiently high energies of the incident nucleon, the cross sections no longer fluctuate wildly but are smooth. The fluctuation cross section then tends to zero $\bar{\sigma}_{fl}=0$. At very low incident nucleon energies where the compound nuclear resonances are very narrow and well separated, $\bar{\sigma}_{fl}$ can be determined by direct evaluation (Feshbach, Porter, and Weisskopf, 1954). In this case, it is just the average compound elastic cross section $\bar{\sigma}_{ce}$. Since compound elastic scattering occurs after the incident nucleon has been removed from the incident channel, it is not described by the optical model.

The behavior of $\bar{\sigma}_{fl}$ and $\bar{\sigma}_{ce}$ has been qualitatively explained by Friedman and Weisskopf (1955). They point out that an incident wave packet may be separated into two parts, one that is undelayed and one that is delayed

by the formation of compound states. The optical model, as a result of the averaging process, regards the delayed component as being removed from the entrance channel whether all or part of it reappears as compound elastic scattering. As the incident nucleon energy increases, the compound lifetime may become so short that no time delay occurs in compound elastic scattering. This is just the statement that $\bar{\sigma}_{fl}$ tends to zero as the energy increases. In this case, σ_{ce} will contribute more and more to $\bar{\sigma}_{se}$ and less and less to $\bar{\sigma}_{c}$. Thus, in the intermediate energy region, the major part of the observed elastic scattering will be the shape elastic scattering predicted by the optical model; but there will be another part resulting from time delayed compound elastic scattering which is not included in the elastic scattering predicted by the model.

2. Form of Potential. The square well shape of the potential originally used by Feshbach, Porter, and Weisskopf (1954) has several shortcomings:

1) The sharp cutoff at the nuclear radius is unrealistic and causes too much reflection at the boundary, especially for high neutron energies. It is more reasonable to assume that the potential shape should resemble the mass distribution shape.
2) Absorption can be expected to occur more readily at the nuclear surface than in the interior. The reason for this is that nucleons near the surface of the nucleus are less inhibited by the Pauli exclusion principle from changing their state and can more readily interact with the incident particle than can nucleons near the center.
3) The success of the shell model in describing nuclear structure suggests that spin orbit coupling may play a role in the scattering process. In this case, the potential should also depend on the angular momentum carried in by the neutron.

4) Using rounded square well potentials, the potential well depths have been found to vary with energy. Perey and Buck (1962) suggest that the energy dependence arises partly because of an intrinsic energy dependence and partly because the effective interaction is non-local. This means that the energy of a particle at point $\vec{r}$ depends not only on $\vec{r}$ but also on the wave function at other points $\vec{r}'$ near $\vec{r}$. More precisely, the energy operator is not diagonal in coordinate space. The Schroedinger equation is therefore

$$-\hbar^2/2m \nabla_r^2 \psi(r) + \int d\vec{r}' V(\vec{r}, \vec{r}') \psi(\vec{r}') = E \psi(\vec{r}) \qquad (10)$$

A potential of this form can be understood as reflecting the correlations in nuclear matter, whereby the presence of a particle at position $\vec{r}$ influences the probability of finding another nucleon at point $\vec{r}'$ in the neighborhood of $\vec{r}$. This in turn affects the energy of the particle at $\vec{r}$ and leads to a potential energy of the form of the integral in Eq. (10). In particular, the form $V(\vec{r}, \vec{r}')$ is chosen on the basis of symmetry between $\vec{r}$ and $\vec{r}'$ to be the product of an average potential strength U and a distribution function H peaked at $\vec{r} = \vec{r}'$:

$$V(\vec{r}, \vec{r}') = U\left(\frac{\vec{r} + \vec{r}'}{2}\right) H\left(\frac{\vec{r} - \vec{r}'}{\beta}\right) \qquad (11)$$

where β is of the order of the range of nuclear forces. Perey and Buck have made the further assumptions that (1) the nucleus is spherical so that the U term is a function of the magnitude of the vector $\vec{r} + \vec{r}'$, and (2) the distribution function may be approximated by a gaussian function:

$$H(\vec{r}, \vec{r}') = \exp \frac{\sum -(\vec{r} - \vec{r}')^2}{\pi^{3/2} \beta^{3/2}} \qquad (12)$$

They have studied the consequences of using such a non-local potential (except for the spin-orbit part, which was local) to see how much energy dependence of the local potentials previously used can be accounted for purely in terms of non-locality. Their results indicate that one set of parameters can give quite good results over a large range of incident neutron energies (0.4 to 2.4 MeV).

These considerations lead to local potentials of the form

$$V = -V_c f(r) - iW_c g(r) + \left(\frac{\hbar}{\mu c}\right)^2 (V_{so} + iW_{so})\left(\frac{df}{r dr}\right)\vec{\sigma}\cdot\vec{\ell} \qquad (13)$$

where V_c, W_c, V_{so}, and W_{so} are energy dependent well depths; $f(r)$ and $g(r)$ give the well shape as a function of r; the operators $\vec{\sigma}$ and $\vec{\ell}$ are the Pauli spin operator and the orbital angular momentum operator divided by $\hbar$ for the incident neutron. The constant $\frac{\hbar}{\mu c}$ is the π-meson Compton wavelength so that $\frac{\hbar}{\mu c}$ is $2*10^{-26}$ cm^2. It is assumed that the well depths are independent of the nature of the target nucleus. The shape functions depend on the radius of the target nucleus, the radius of the potential varying in direct proportion to the nuclear radius. A form for $f(r)$ that has had considerable success is the Woods-Saxon (1954) form

$$f(r) = \left[1 + \exp\left(\frac{r-R}{d}\right)\right]^{-1}$$

with $R = r_0 A^{1/3}$ greater than the value for the charge distribution. Since the neutron and proton distributions are essentially the same, the difference in radii must be interpreted as an effect of the finite force range.

Two different assumptions have been made about the absorption term:

(a) Volume absorption $\qquad g(r) = f(r)$

(b) Surface absorption $\qquad g(r) = \exp\left[-\frac{(r-R)^2}{b^2}\right]$ or $g(r) = \frac{d}{dr}\left[1 + \exp\left(\frac{r-R}{b}\right)\right]^{-1}$

The latter form is purely phenomenological, and b is an adjustable parameter. With assumption (a), V(r) has six parameters; with assumption (b) it has seven, although in practice W_s is always negligible.

The introduction of spin-orbit coupling also complicates formulas (8) and (9). When there is spin-orbit force, the states $j = l \pm 1/2$ have different phase shifts. Introducing phase shifts ξ_l^+ corresponding to $j = l + 1/2$ and ξ_l^- corresponding to $j = l - 1/2$, formulas (8) and (9) become

$$\left(\frac{\overline{d\sigma}}{d\Omega}\right)_{se} = |A|^2 + |B|^2$$

$$A = -\left(\frac{i\lambda}{2}\right) \sum_l \{(l+1)(e^{2i\xi_l^+} - 1) + l(e^{2i\xi_l^-} - 1)\} P_l(\cos\theta)$$

$$B = -\left(\frac{\lambda}{2}\right) \sum_l (e^{2i\xi_l^+} - e^{2i\xi_l^-}) P_l^1(\cos\theta)$$

$$P_l^1 = \sin\theta \left[\frac{d}{dx} P_l(x)\right]$$

$$\overline{\sigma}_{se} = 4\pi\lambda^2 \sum_l \{(l+1)[e^{-2\phi_l^+} \sin^2\rho_l + 1/4 (1 - e^{-2\phi_l^+})^2] + l[e^{-2\phi_l^-} \sin^2\rho_l + 1/4 (1 - \exp[-2\phi_l^-])^2\}$$

$$\overline{\sigma}_c = \pi\lambda^2 \sum_l \{(l+1)(1 - e^{-4\gamma_l^+}) + l(1 - e^{-4\gamma_l^-})\}$$

$$= \pi\lambda^2 \sum_l \{(l+1) T_l^+ + l T_l^-\}$$

C. Inelastic Scattering

We begin by describing a general expression derived by Blatt and Biedenharn (1952) for the differential cross section for the emission of reaction products due to the bombardment of a target nucleus by a mono-energetic beam of unpolarized neutrons. Their result, corrected by Huby is

$$\frac{d\sigma}{d\Omega}(\alpha'|\alpha) = \frac{\lambda^2}{8}\frac{(-)^{s-s'}}{2I+1} Z(\ell_1 J_1 \ell_2 J_2 ; sL) Z(\ell_1' J_1 \ell_2' J_2 ; s'L) \cdot \tag{16}$$

$$Re\, J(\alpha'\ell_1' s'|\alpha\ell_1 s|J_1\pi_1) J^*(\alpha'\ell_2' s'|\alpha\ell_2 s|J_2\pi_2) P_L(\cos\theta)$$

The subscript α denotes all the numbers necessary to specify the initial system; such as the center of mass energy E, while the subscript α' denotes the state of the residual nucleus and the type of particle emitted. Since the total angular momentum is conserved in any process, the cross section has been decomposed according to possible values of the total angular momentum J. The total angular momentum is composed of the sum of the intrinsic spin of the target and projectile (or residual nucleus and emitted particle) together with the orbital angular momentum ℓ of the system.

$$\vec{J} = \vec{I} + \vec{\ell} + \vec{i} = \vec{I}' + \vec{\ell}' + \vec{i}'$$

The channel spin appearing in the equation is composed of the intrinsic spins of the reacting particles.

$$\vec{S} = \vec{I} + \vec{i}$$

$$\vec{J} = \vec{\ell} + \vec{S}$$

For unpolarized beams, $\vec{S}$ is random so that evaluation of the cross section involves averaging over all possible orientations of $\vec{S}$. The angle between the emitted particle and the incident beam is given by θ. The transition

matrix for an intermediate state with total angular momentum J and parity π describing the transition from state α channel spin $\vec{S}$ to state α' channel spin $\vec{S}'$, the incident particle having an orbital angular momentum ℓ' is denoted by $\mathcal{J}(\alpha \ell S | \alpha' \ell' S' | J \pi)$.

The probability of forming a state of total angular momentum J_1 from ℓ_1 and S or J_2 from ℓ_2 and S is given by $\bar{Z}(\ell_1 J_1 \ell_2 J_2 ; S L)$. Thus, the $\bar{Z}$ factors are kinematical in the sense that they do not depend upon the nature of nuclear interactions but only upon the details of the decomposition of the initial plane wave into states of a given J, π, ℓ, and S, and upon the decay of this system into various possible final values of ℓ' and S'. In terms of the Racah and Clebsch-Gordan coefficients

$$\bar{Z}(\ell_1 J_1 \ell_2 J_2 ; S L) = [(2\ell_1+1)(2J_1+1)(2\ell_2+1)(2J_2+1)]^{1/2} \times (\ell_1 \ell_2 00 | L 0)\, W(\ell_1 J_1 \ell_2 J_2 ; S L) \qquad (17)$$

The dynamics of the problem are contained in the elements of the transition matrix $\mathcal{J}$.

1. Hauser-Feshbach Formula. In order to simplify Eq. (16) and put it in a form containing values which can be calculated, we make four assumptions about the reaction process by which the scattering takes place:

1) The scattering takes place by the formation and subsequent decay of the compound nucleus.
2) As in the case of an isolated compound resonance, the contribution of each total angular momentum and parity of the system to the scattering cross section may be factored into a partial compound nucleus formation cross section and an independent decay probability for each open exit channel.

3) The statistical model holds for the compound nucleus so that interference terms between partial waves with different ℓ values resulting from the decay of states with the same J value will drop out in the summation.

With these assumptions, Eq. (16) becomes

$$\frac{d\sigma}{d\Omega}(\alpha|\alpha') = \frac{\lambda^2}{8}\sum(-)^{s-s'}\bar{Z}(\ell J \ell J; sL)\bar{Z}(\ell' J \ell' J; s' L)\cdot$$

$$|\bar{\mathcal{J}}_f(\alpha \ell s | J\pi)|^2 |\mathcal{J}_d(\alpha' \ell' s' | J\pi)|^2 P_L(\cos\theta) \qquad (18)$$

where, in accordance with assumption (3), we have omitted the subscripts 1 and 2 on the ℓ and J values appearing in the formula. In order to explicitly show the resultant independence of the formation and decay of each compound state of a given parity π and total angular momentum J, we have written $|\mathcal{J}(\alpha \ell s|\alpha' \ell' s'|J\pi)|^2$ as $|\bar{\mathcal{J}}_f|^2|\bar{\mathcal{J}}_d|^2$ where $\mathcal{J}_f$ is the transition matrix for formation of the compound nucleus and $\mathcal{J}_d$ is the transition matrix for its decay. Since many levels are excited simultaneously, we replace $\mathcal{J}$ by $\bar{\mathcal{J}}$ where the bar indicates an energy average over levels with the same J and π. Since the factor contains only the dynamics of the compound nucleus formation, we may write $|\bar{\mathcal{J}}_f|^2 = T_\ell^J(E)$ where $T_\ell^J(E)$ is a transmission coefficient or "sticking probability" representing the probability that a neutron incident in channel α with angular momentum ℓ and energy E will be absorbed to form a compound state of spin J. According to the reciprocity theorem, the probability for decay of the compound nucleus into a given channel can be calculated in the same way that the formation probability was determined. If there are many open channels, then the probability for decay into any one of them will be given by the branching ratio

$$T_{\ell'}^J(E')/\sum T_{\ell''}^J(E'') \qquad (19)$$

where $\sum T_{\ell''}^{J}(E)$ is a sum of transmission coefficients for all competing channels α'' into which the neutron can be emitted while conserving energy, parity, and angular momentum. Thus, finally we have

$$\frac{d\sigma}{d\Omega}(\alpha|\alpha') = \frac{\lambda^2}{8} \sum' \frac{(2J+1)}{(2I+1)} (-)^{s-s'} Z(\ell J \ell' J' s L) Z(\ell J \ell' J' s' L) P_L(\cos\theta) \frac{T_{\ell' s'}^{J} T_{\ell s}^{J}}{\sum T_{\ell'' s''}^{J}} \qquad (20)$$

The corresponding integrated cross section is

$$\sigma(\alpha|\alpha') = \pi\lambda^2 \sum' \frac{(2J+1)}{(2I+1)} T_{\ell s}^{J} T_{\ell' s'}^{J} / \sum T_{\ell'' s''}^{J} \qquad (21)$$

This is the well known result of Hauser and Feshbach (1952). If the compound nucleus formation cross section may be identified with the corresponding optical model cross section, then the transmission coefficients may be calculated using Eq. (7).

The Hauser-Feshbach formula has enjoyed great popularity among experimental workers because its parameters are all relatively easily calculable, being either purely "geometrical" in nature or obtainable from optical model calculations; and its predictions have, in most cases, agreed well with experimental measurements of neutron inelastic scattering.

However, careful examination of the assumptions underlying the derivation of the formula have led to the introduction of a number of modifications. The nature of these modifications depends primarily on the ratio of $\langle \Gamma^{J\pi} \rangle / D_{J\pi}$ where $\langle \Gamma^{J\pi} \rangle$ is the average total width of states with a given angular momentum J and parity π, and $D_{J\pi}$ is the average spacing between levels with the same J and π at the excitation energy of the compound system.

2. Widely Spaced Levels. Before proceeding further, we simplify our notation by introducing a more general "channel" subscript such that

$$c \equiv (\alpha \ell s \mid J\pi)$$

and a double subscript cc' denoting transitions between the initial and final channels such that

$$cc' \equiv (\alpha' \ell' s' \mid \alpha \ell s \mid J\pi)$$

In the limit of $\langle \Gamma^{J\pi} \rangle \ll D_{J\pi}$, the scattering cross section can be written as a sum over single level Briet-Wigner terms. Using our new notation

$$\sigma_{\alpha\alpha'} = \sum_{cc'} \sigma_{cc'}$$

$$\sigma_{cc'} = \pi \lambda^2 \frac{(2J+1)}{2(2I+1)} \sum_{\lambda} \frac{\Gamma_{\lambda c} \Gamma_{\lambda c'}}{(E_\lambda - E)^2 + \frac{1}{4}\Gamma_\lambda^2} \qquad c \neq c' \tag{22}$$

The average of $\sigma_{cc'}$ over an energy interval ΔE

$$\langle \sigma_{cc'} \rangle_{\Delta E} = \frac{1}{\Delta E} \int_{\Delta E} \sigma_{cc'} \, dE$$

is easily evaluated under the assumption that the resonance statistics are uniform from $-\infty$ to $+\infty$ and one obtains:

$$\langle \sigma_{cc'} \rangle_{\Delta E} = 2\pi \lambda_c^2 \frac{(2J+1)}{2(2I+1)} \frac{1}{\Delta E} \sum_{\lambda} \frac{\Gamma_{\lambda c} \Gamma_{\lambda c'}}{\Gamma_\lambda}$$

$$= 2\pi^2 \lambda_c^2 \frac{2J+1}{2(2I+1)} \frac{1}{D_{J\pi}} \left\langle \frac{\Gamma_{\lambda c}^{J\pi} \Gamma_{\lambda c'}^{J\pi}}{\Gamma^{J\pi}} \right\rangle \tag{23}$$

In order to obtain the Hauser-Feshbach formula, the assumption must be made that

$$\left\langle \frac{\Gamma_{\lambda c}^{J\pi} \Gamma_{\lambda c'}^{J\pi}}{\Gamma^{J\pi}} \right\rangle = \left[\frac{\langle \Gamma_{\lambda c}^{J\pi} \rangle \langle \Gamma_{\lambda c'}^{J\pi} \rangle}{\langle \Gamma^{J\pi} \rangle} \right] \tag{24}$$

Below, we derive the relation $T_c = \frac{2\pi}{D}\langle \Gamma_c \rangle$ for $\Gamma_c \ll D$. Using this, we obtain the original Hauser-Feshbach term

$$\frac{\langle \Gamma_{\lambda c} \rangle \langle \Gamma_{\lambda c'} \rangle}{\langle \Gamma \rangle} = \frac{T_c T_{c'}}{\sum T_{c''}} \tag{25}$$

In this limit of $\langle \Gamma^{J\pi} \rangle \ll D_{J\pi}$, the assumption (24) essentially amounts to assuming that complete positive correlation holds between different partial widths with the same values of α , l , s ; i.e.,

$$\frac{\Gamma_{\lambda c}}{\langle \Gamma_{\lambda c} \rangle_\lambda} = \frac{\Gamma_{\lambda c'}}{\langle \Gamma_{\lambda c'} \rangle_\lambda} \tag{26}$$

Direct experimental evidence has been accumulated in recent years that indicates that the partial widths are not completely correlated. In addition, evidence about the distribution of the widths has been obtained. These experiments were performed with neutrons of low energy (some tens of electron volts) with the tentative conclusions which we take from the analysis of Porter and Thomas (1956) that the distributions of neutron widths obeys the following law where $P(\Gamma)d\Gamma$ is the probability that the value of the width will fall between Γ and $\Gamma + d\Gamma$

$$P(\Gamma)\, d\Gamma = \frac{1}{\sqrt{2\pi}} \frac{e^{-x/2}}{\sqrt{x}}\, dx \quad , \qquad x = \Gamma/\langle \Gamma \rangle \tag{27}$$

Here $\langle \Gamma \rangle$ is the average value of Γ :

$$\langle \Gamma \rangle = \int_0^\infty \Gamma\, P(\Gamma)\, d\Gamma$$

We note that small widths are favored but that the dispersion is very large:

$$\delta = \frac{\langle \Gamma^2 \rangle - \langle \Gamma \rangle^2}{\langle \Gamma \rangle^2} = 2$$

That is, the distribution $P(\Gamma)$ is very broad.

The observed distribution of the spacing of energy levels is consistent with the Wigner distribution (Wigner, 1956)

$$P(S)dS = \frac{\pi}{2D^2} S e^{-\pi/4 S^2/D^2} dS \qquad (28)$$

where D is the average spacing of the levels. The dispersion in this case is

$$\delta = \frac{\langle S^2 \rangle - D^2}{D^2} = \frac{4}{\pi} - 1$$

These results, by their very form, suggest that there is a random character present in the description of nuclear reactions.

Lane and Lynn (1957) and Dresner (1957) calculated the correction that should be made to the Hauser-Feshbach formula under the following assumptions:

1) The cross section is correctly described by equation (16)
2) The partial widths are uncorrelated.
3) The partial widths follow a Porter-Thomas distribution.
4) The partial widths may be replaced by optical model transmission coefficients using the relation

$$T_\ell(E) = \frac{2\pi}{D_{J\pi}} \langle \Gamma^{J\pi}_{\lambda c \ell} \rangle_\lambda \qquad (29)$$

Note that for simplicity, Dresner ignored any possible dependence of T on the angular momentum J .

$$\sigma_{\alpha\alpha'} = \frac{\pi\lambda^2}{2(2I+1)} \sum_{J\pi\ell s s'} (2J+1) \left\langle \frac{T_\alpha T_{\alpha'}}{\sum_{\alpha''} T_{\alpha''}} \right\rangle$$

$$= \frac{\pi\lambda^2}{2(2I+1)} \sum_{J\pi\ell\ell'} (2J+1) \left\langle \frac{\epsilon_{J\ell} T_\ell(E) \, \epsilon_{J\ell'} T_{\ell'}(E')}{\sum_{\ell''} \epsilon_{J\ell''} T_{\ell''}(E'')} \right\rangle \qquad (30)$$

where the $\epsilon_{J\ell}$ equal the number of values of channel spin that take part in each transition through the compound state $J\pi$ for orbital angular momentum ℓ . Then

$$\sigma_{\alpha\alpha'} = \frac{\pi\lambda^2}{2(2I+1)} \sum_{J\pi\ell\ell'} (2J+1) \frac{\epsilon_{J\ell} T_\ell(E) \, \epsilon_{J\ell'} T_{\ell'}(E')}{\sum_{\ell''} \epsilon_{J\ell''} T_{\ell''}(E'')} R_{\alpha\alpha'}^{J\ell\ell'} \qquad (31)$$

where $R_{\alpha\alpha'}^{J\ell\ell'}$ is Dresner's "width fluctuation correction factor" resulting from the assumed Porter-Thomas distribution of partial widths. It may be written

$$R_{\alpha\alpha'}^{J\ell\ell'} \cong \left(\sum_{\ell''} \epsilon_{J\ell''} T_{\ell''}(E'')\right) \int_0^\infty (1 + 2T_\ell(E))^{-\left(\frac{\epsilon_{J\ell}}{2} + 1\right)}$$

$$\cdot (1 + 2T_{\ell'}(E')x)^{-\left(\frac{\epsilon_{J\ell}}{2} + 1\right)} \prod_{\ell'' \neq \ell\ell'} (1 + 2T_{\ell''}(E''')x)^{-\frac{\epsilon_{J\ell''}}{2}} dx \qquad (32)$$

The correction is largest when there are only a few competing channels. In fact, for only two channels with equal average widths, one obtains a maximum

fluctuation effect of

$$R = \frac{\langle \Gamma_{\lambda c} \Gamma_{\lambda c'} / (\Gamma_{\lambda c} + \Gamma_{\lambda c'}) \rangle}{\langle \Gamma_{\lambda c} \times \Gamma_{\lambda c'} \rangle / \langle \Gamma_{\lambda c} + \Gamma_{\lambda c'} \rangle} = 1/2 \qquad (33)$$

For $c = c'$ R has the value 2. In fact, the width fluctuation correction always is found to enhance compound elastic scattering at the expense of inelastic scattering.

As the number of competing channels increases, the value of R approaches unity. In this case, however, the value of $\langle \Gamma^{J\pi} \rangle / D_{J\pi}$ also increases so that the expansion (22) is no longer valid.

As the excitation of the compound system increases, the ratio of level width to spacing increases rapidly. As the levels begin to overlap, the cross section is simultaneously dominated by a large number of reasonances. Then, it is no longer possible to expand the reaction cross section as a sum over single-level Breit-Wigner resonances. In the case where $\langle \Gamma^{J\pi} \rangle \gg D_{J\pi}$ the cross section can be obtained by making suitable assumptions about the scattering matrix. Following Moldauer (1963) and Ericson (1963), we assume that in a suitable energy interval the scattering matrix can be represented by

$$\mathcal{J}_{cc'} = \mathcal{J}_{cc'}^{direct} + \mathcal{J}_{cc'}^{fluct} \qquad (34)$$

where $\mathcal{J}_{cc'}^{direct}$ is very slowly varying in the interval. It includes the effects of nuclear potential scattering as well as processes which may be discussed in terms of direct reaction models such as the distorted wave Born approximation. We identify $\mathcal{J}_{cc'}^{fluct}$ with the random part of the scattering amplitude.

According to Feshbach's unified theory (Feshbach, 1962), it may be written

$$\mathcal{T}_{cc'}^{fluct} = i\, e^{i(\delta_c + \delta_{c'})} \sum_{\lambda} \frac{a_\lambda}{(E - E_\lambda)} \tag{35}$$

where $a_\lambda = \gamma_{c\lambda}\gamma_{\lambda c'}$ is a product of the width amplitudes leading from the initial state c to the final state c' and E_λ is the rapidly varying complex energy $E_\lambda = Re\, E_\lambda - i\Gamma_\lambda/2$. In terms of the scattering matrix, the energy averaged reaction cross section may be written

$$\langle \sigma_{cc'} \rangle = \pi \lambda^2 \langle | \mathcal{T}_{cc'} |^2 \rangle \tag{36}$$

which may be separated into the following four terms

$$\begin{aligned}
\sigma_{cc'}^{direct} &\equiv \pi \lambda_c^2 \, | \mathcal{T}_{cc'}^{direct} |^2 \\
\sigma_{cc'}^{correlation} &\equiv \pi \lambda_c^2 \, | \langle \mathcal{T}_{cc'}^{fluct} \rangle |^2 \\
\sigma_{cc'}^{fluct} &\equiv \pi \lambda_c^2 \langle | \mathcal{T}_{cc'}^{fluct} - \langle \mathcal{T}_{cc'}^{fluct} \rangle |^2 \rangle \\
\sigma_{cc'}^{interf} &\equiv \pi \lambda_c^2 \, 2 Re\, \mathcal{T}_{cc'}^{direct\,*} \langle \mathcal{T}_{cc'}^{fluct} \rangle
\end{aligned} \tag{37}$$

These expressions may be simplified if we assume that the width amplitudes are uncorrelated for $\lambda \neq \lambda'$ and that they are normally distributed and are positive or negative with equal probability. The second assumption is justified as follows: It has been shown by Porter and Blumberg (1958) that both equations (27) and (28) follow from the assumption that the matrix elements of the Hamiltonian, whose eigenvalues and eigenvectors are the energy levels and wave functions of the compound nucleus, are random, their

~~distrubtion~~ distribution being gaussian. One important corollary of this is that the width amplitudes $\gamma_{\lambda c}$ have a gaussian distribution of widths and that they are positive or negative with equal probability. With these assumptions, the non-diagonal terms will cancel in the summation of Eq. (35), and we will have

$$\langle \mathcal{J}_{cc'}^{fluct} \rangle = 0$$

which leads to

$$\sigma_{cc'}^{correl} = 0$$

$$\sigma_{cc'}^{interf} = 0 \qquad (38)$$

and

$$\langle \sigma_{cc'}^{fluct} \rangle = \frac{2\pi\lambda^2}{D J\pi} \left\langle \frac{|\gamma_{\lambda c}|^2 \, |\gamma_{\lambda c'}|^2}{\Gamma_\lambda} \right\rangle_\lambda \qquad (39)$$

In terms of the $\gamma_{\lambda c}$, the partial widths $\Gamma_{\lambda c}$ may be written

$$\Gamma_{\lambda c} = |\gamma_{\lambda c}|^2 / N_\lambda$$

where N_λ is a real normalization constant $N_\lambda \geq 1$ such that

$$\Gamma_\lambda = \sum_c \Gamma_{\lambda c}$$

Using these expressions in Eq. (39), we have

$$\langle \sigma_{cc'}^{fluct} \rangle = \frac{2\pi\lambda^2}{D} \left\langle \frac{\Gamma_{\lambda c} \, \Gamma_{\lambda c'}}{\Gamma_\lambda} \right\rangle_\lambda \qquad (40)$$

We thus have once again, in the limit of $\Gamma \gg D$, the "Dresner" formula obtained previously on the assumption that $\Gamma \ll D$. As noted above,

the ratio

$$\left\langle \frac{\Gamma_{\lambda c}\,\Gamma_{\lambda c'}}{\Gamma_\lambda} \right\rangle \Big/ \frac{\langle \Gamma_{\lambda c}\rangle \langle \Gamma_{\lambda c'}\rangle}{\langle \Gamma_\lambda \rangle} \tag{41}$$

approaches unity for many open channels and $\langle \Gamma^{J\pi} \rangle \gg D_{J\pi}$. Thus, using the relation

$$T_c = \frac{2\pi}{D} \langle \Gamma_{\lambda c} \rangle_\lambda \tag{42}$$

we have

$$\langle \sigma_{cc'}^{fluct} \rangle = \pi \lambda\!\!\!^{-2} \frac{T_c\, T_{c'}}{\sum_{c''} T_{c''}} \tag{43}$$

To obtain the "observed" reaction cross section, we sum over channels c' and average over channels c

$$\langle \sigma_{\alpha\alpha'}^{fluct} \rangle = \frac{\pi \lambda\!\!\!^{-2}}{2(2I+1)} \sum (2J+1) \frac{T_c\, T_{c'}}{\sum_{c''} T_{c''}} \tag{44}$$

which is the original Hauser-Feshbach formula. We emphasize that our results are true only for $\Gamma \gg D$ and $\Gamma \ll D$. In the intermediate region, $\Gamma \approx D$ higher order terms appear in Eq. (39), and the resulting formulas for the cross sections contain parameters that are, at present, completely inaccessible.

The correspondence between the optical model transmission coefficient T_c and the ratio $\langle \Gamma_c / D_J \rangle$ can be obtained by taking the energy average of the scattering matrix $\mathcal{J}_{cc}$. The result is

$$\langle \mathcal{J}_{cc} \rangle = 1 - \exp[2i\delta_c] + \pi \exp[2i\delta_c] \left\langle \frac{\Gamma_{c\lambda}^{J\pi}}{D_{J\pi}} \right\rangle_\lambda$$
$$\delta_c = \alpha + i\beta \tag{45}$$

By identifying this with the optical model scattering amplitude

$$\langle \mathcal{J}_{cc} \rangle = 1 - \eta_\ell \tag{46}$$

and using the relation

$$T_c = 1 - |\eta_\ell|^2 \tag{47}$$

we find

$$T_c = 1 - \exp[-4\beta_c]\left(1 - \pi \left\langle \frac{\Gamma_{\lambda c}}{D_J} \right\rangle_\lambda\right)^2 \tag{48}$$

For $\langle \Gamma^{J\pi} \rangle \ll D_{J\pi}$ we have

$$T_c \cong 2\pi \left\langle \frac{\Gamma_{c\lambda}^{J\pi}}{D_{J\pi}} \right\rangle_\lambda \exp[-4\beta_c] \tag{49}$$

Note that the phase shift δ_c of the scattering matrix $\mathcal{J}_{cc'}$ (which should not be identified with the optical model phase shift ξ) is complex if the determining potential produces changes in channel spin or angular momentum or if direct reactions are present. This may become important as the bombarding energy increases. We have assumed in the expressions above relating partial widths and transmission coefficients that $\beta \cong 0$.

3. Magnitudes of Fluctuations. The quantities discussed so far have been average quantities. Naturally, there will be large fluctuations away from these averages. Ericson (1963) has attempted to describe the average behavior of these fluctuations in the region of overlapping levels. He proceeds in a fashion similar to that used in deriving expressions for the

average cross sections, making the same assumption about the random distribution of the reduced widths. His results are applicable only for the case $\langle \Gamma^{J\pi} \rangle \gg D_{J\pi}$. The results for $\langle \Gamma^{J\pi} \rangle \approx D_{J\pi}$ are much more complicated than the ones described below. He defines a correlation function for the cross section

$$F(\epsilon) = \langle (\sigma(E+\epsilon) - \langle \sigma \rangle)(\sigma(E) - \langle \sigma \rangle) \rangle \tag{50}$$

In the case of $\epsilon = 0$, the correlation function is simply the energy average of the square of the fluctuation in the cross section

$$F(0) = \langle (\delta \sigma(E))^2 \rangle \tag{51}$$

Ericson has evaluated this function in the simple case where no angular momentum effects are taken into account. His result is

$$F_{cc'}(E) = \frac{1}{1+(\epsilon/\Gamma)^2} \langle \sigma_{cc'} \rangle^2 \tag{52}$$

The Lorentzian factor $[1 + (\epsilon/\Gamma)^2]^{-1}$ is due to the fact that the intermediate compound system is on the average decaying exponentially at a rate $\hbar/\Gamma$. It expresses the fact that the uncertainty in energy of an intermediate state λ causes it to contribute to reactions which may differ in energy from the resonant energy by an amount of the order Γ . This introduces correlations in the cross section over such energy intervals and provides a crude means for measuring the average total width over an energy interval in the continuum region where the individual resonances cannot be directly observed.

For the case where angular momentum effects are taken into account, Ericson obtains analogous but much more complicated expressions for the

fluctuations in the cross sections. We mention here only a few of his results. For a particular reaction, the correlation function is given by

$$\langle(\sigma_{\alpha\alpha'}(E+\epsilon)-\langle\sigma_{\alpha\alpha'}\rangle)(\sigma_{\alpha\alpha'}(E)-\langle\sigma_{\alpha\alpha'}\rangle)\rangle = \left[\frac{\pi\lambda^2}{(2i+1)(2I+1)}\right]^2 \cdot \sum_{cc'}(2J+1)^2\frac{\Gamma_J^2}{\epsilon^2+\Gamma_J^2}\left(\frac{T_c\,T_{c'}}{\sum_{c''}T_{c''}}\right)^2 \tag{53}$$

The corresponding correlation function for the total cross section is given by

$$\langle(\sigma_\alpha(E+\epsilon)-\langle\sigma_\alpha\rangle)(\sigma_\alpha(E)-\langle\sigma_\alpha\rangle)\rangle = 2\left(\frac{\pi\lambda^2}{(2i+1)(2I+1)}\right)^2\sum_c(2J+1)^2\frac{\Gamma_J^2}{\epsilon^2+\Gamma_J^2}\frac{T_c^2}{\sum_{c'}T_{c'}} \tag{54}$$

He evaluates

$$R_{\alpha\alpha'} \equiv (F_{\alpha\alpha'}(\epsilon=0))/\langle\sigma_{\alpha\alpha'}\rangle^2 = \frac{\langle(\sigma_{\alpha\alpha'}(E)-\langle\sigma_{\alpha\alpha'}\rangle)^2\rangle}{\langle\sigma_{\alpha\alpha'}\rangle^2} = \frac{\sum(2J+1)^2\left(T^J_{\alpha s\ell}\,T^J_{\alpha' s\ell}\right)^2}{\left(\sum(2J+1)\,T^J_{\alpha s\ell}\,T^J_{\alpha s\ell}\right)^2} \tag{55}$$

We observe that this ratio is always smaller than unity since all terms in the denominator are positive and those in the numerator are exactly the diagonal terms in the expansion of the square in the denominator.

He obtains similar expressions for the fluctuations in the angular distributions. These fluctuations may give rise to assymetries about 90° in the angular distributions and cause variations in the amount of anisotropy. His results indicate that much larger fluctuations should be expected in the angular distributions than in the integrated cross section. This can be seen simply by noting that the angle integrated cross section is proportional only

to the $\ell=0$ term in the partial wave expansion of the angular distribution. Hence, only the fluctuations in this term will contribute to the fluctuations in the integrated cross section. In particular, for the case of all spins zero and the initial and final parity the same he obtains exactly

$$\frac{\langle (d\sigma_{\alpha\alpha'}/d\Omega - \langle d\sigma_{\alpha\alpha'}/d\Omega \rangle)^2 \rangle}{\langle d\sigma_{\alpha\alpha'}/d\Omega \rangle^2} = 1 \qquad (56)$$

Thus, for a statistical zero spin reaction, the relative fluctuations in the differential cross section are unity independent of dynamical factors. He finds that the fluctuations are damped by spins of projectiles and target nuclei, however. Therefore, this expression represents the limiting value for the fluctuations in the angular distributions.

It is important to examine how well the silicon and sulfur nuclei may be expected to fit the models we have discussed at the bombarding energies used in this experiment.

D. Applicability of Models

1. Elastic Scattering. The optical model parameters used in the calculations were determined by fitting data on heavy elements (^{208}Pb). Using these parameters, the model has accurately described a wide variety of data on heavy elements. However, for nuclei with $A \lesssim 20$, the fits have generally been found to give qualitative agreement but not the excellent quantitative agreement that is found for heavier elements. For very light nuclei (e.g. carbon), the agreement between optical model predictions and experiment is very poor. The reason for this is presumably that for light elements with few nucleons, the picture

of an incident nucleon interacting with a smooth average potential due to all the nucleons in the nucleus is not valid.

Therefore, because of their light weight, the silicon and sulfur elastic scattering angular distributions should not be expected to agree precisely with the optical model predictions.

However, some improvement in agreement between theory and experiment might be expected if the potential well depths are slightly reduced from the previously determined values. This is suggested by the fact that the overall density of nuclear matter in light nuclei is less than the density in the heavier elements for which the optical model parameters were determined. Thus, the optical potential strength might be correspondingly less.

At the lower bombarding energies used in this experiment, large fluctuations appear in the cross sections. Since the optical model is designed to predict cross sections averaged over energy, no amount of adjustment of the parameters can be expected to produce precise agreement between theory and experiment in this region.

2. Inelastic Scattering. In our discussion of inelastic scattering, we began by invoking the statistical model which, in essence, simply requires that many levels in the compound nucleus be excited simultaneously. More careful analysis has shown, however, that the formulas for describing inelastic scattering depend not only on the statistical model assumption but also on the magnitude of $\langle \Gamma^{J\pi} \rangle / D_{J\pi}$. The formulas predict the cross sections correctly only in the two extreme cases where $\langle \Gamma^{J\pi} \rangle \ll D_{J\pi}$ and $\langle \Gamma^{J\pi} \rangle \gg D_{J\pi}$. Moreover, we have seen that even in the limiting case of $\langle \Gamma^{J\pi} \rangle \gg D_{J\pi}$ there will be large fluctuations in the cross sections. Thus, the primary assumption of the statistical model, namely that many levels be simultaneously

excited, at most causes partial waves with different ℓ values due to decay of compound states with the same J, π to cancel in the summations of Eq. (16) so that the angular distributions will be symmetric about 90°. Once again, however, large fluctuations away from the symmetric angular distributions can be expected even when the statistical assumption is satisfied.

Let us first consider whether, at the bombarding energies used in the experiment, enough levels are excited to satisfy the primary assumptions of the statistical model. Fig. 1 gives an idea of the average level spacing in ^{29}Si and ^{33}S at the excitation energies corresponding to the incident neutron energies used in taking angular distributions. If we assume that the exponential extrapolation shown in the curve for ^{29}Si is approximately correct, the average spacing at the excitations corresponding to an incident neutron energy of 2.6 MeV is about 10 keV. At this energy, the energy spread due to the thickness of the H-Zr target used in taking the angular distributions is about 100 keV, enough to excite about 10 levels in the compound nucleus. This is obviously too few levels to completely fulfill the requirements necessary for the statistical model to hold. Nevertheless, it is hoped that enough levels are excited to make the statistical assumption a reasonable approximation. However, at 4 MeV incident neutron energy, the energy spread was more than 500 keV and the level spacing is estimated to be about 4 keV. Thus, on the order of a hundred levels are involved and the statistical assumption should be quite valid at this energy.

As for the question of whether $\langle\Gamma\rangle \gg D$, this is more difficult to ascertain. We have noted that the Lorentzian factor in Eq. (52) introduces correlations in the cross sections over energy intervals comparable to the average total width in the compound system. Thus, the fluctuations in the cross sections will have periods roughly equal to these intervals. A crude

survey of the periods of the fluctuations in the total cross section curve for silicon indicates that the average of these is at least on the order of 100 keV. If we assume that these fluctuations are of the Ericson type then this would indicate an average total width which is also on the order of 100 keV. If this is true, and our assumed level spacing is approximately correct, then the assumption that $\langle \Gamma^{J\pi} \rangle \gg D_{J\pi}$ is satisfied for all bombarding energies. Obviously, however, we have implicitly assumed that $\langle \Gamma^{J\pi} \rangle \gg D_{J\pi}$ in making our estimate of the average total width. If $\langle \Gamma^{J\pi} \rangle \approx D_{J\pi}$, then the average period of the fluctuations can no longer be used as a criterion for determining the average total width and the argument breaks down. Therefore, at least at the lower bombarding energies, the ratio of $\langle \Gamma^{J\pi} \rangle / D_{J\pi}$ will have to be left as an open question.

In any case, we have made our calculations on the assumption that $\langle \Gamma^{J\pi} \rangle \gg D_{J\pi}$. If this is not true, we can expect other terms to appear in the cross section expressions which will invalidate our results. In particular, Moldauer has pointed out that in the intermediate case of $\langle \Gamma^{J\pi} \rangle \approx D_{J\pi}$, it is not correct to use the optical model transmission coefficients in calculating either the Hauser-Feshbach formula or the width fluctuation correction factor. In this case, the distribution of level spacings must be taken into account and when this is done it has the effect of reducing the values of the transmission coefficients used in the Dresner formula while increasing the calculated cross sections. Unfortunately, there is no way to determine the distributions of the level spacings in this region. However, by making reasonable assumptions about the distribution of level spacings, Moldauer has calculated a number of inelastic scattering cross sections. The cross sections thus calculated generally have values between those calculated using optical model transmission coefficients in the Hauser-Feshbach formula and the Dresner formula.

Referring to Fig. 1, we see that for ^{33}S the average level spacing at an incident neutron energy of 2.6 MeV is apparently about 50 times smaller than the spacing in ^{29}Si. If this is correct, then the statistical assumption should hold very well at all bombarding energies.

There is also reason to believe that the total widths are larger in ^{33}S than in ^{29}Si at the same excitation energies. The reason for this is that there are many more decay channels open to ^{33}S than ^{29}Si. Even at the lowest bombarding energy, the $^{32}S(n,p)$ and $^{32}S(n,\alpha)$ cross sections are appreciable. This is shown in Table I which lists the cross sections for all competing processes at the bombarding energies at which angular distributions were taken. The presence of the large (n,p) and (n,α) cross sections are explained as follows: The thresholds for both these reactions are very low. The (n,α) reaction is exoergic, having a Q value of 1.5 MeV, and the (n,p) reaction is only slightly endoergic, having a Q value of -900 keV. Moreover, the level densities in the residual nuclei, ^{29}Si and ^{32}P, are much larger than in ^{32}S. For example, at an incident neutron energy of 4 MeV there are roughly 15 levels which can be excited in ^{29}Si and ^{32}P by the emission of alphas and protons, whereas only three levels in ^{32}S can be excited if neutron scattering occurs. Each of these excited states represents an open decay channel. The comparatively large number of open channels available for proton or alpha emission makes these reactions statistically far more probable than neutron emission, nullifying the inhibiting effect of the Coulomb barrier, so that even at an incident neutron energy of 2.45 MeV, the (n,p) and (n,α) cross sections are comparable to the (n,n') cross section. The presence of these competing reactions assures that $\Gamma_\lambda = \sum_c \Gamma_{\lambda c}$ will be larger for sulfur than for silicon. At the same time, however, their presence invalidates the predictions of the Hauser-Feshbach and Dresner formulas which

Table I. Summary of Cross Section Data

E_n	σ_T	σ_{nn}	$\sigma_{nn'}$	$\sigma_{n\alpha}$	σ_{np}	$\sigma_{nn'}$(HF)	$\sigma_{nn'}$(Dres.)
			Sulfur				
2.45	2.80	2.39	----	----	0.08	----	----
2.85	3.20	2.80	----	----	0.10	----	----
4.00	2.90	1.87	0.39	0.25	0.20	0.79	0.48
4.90	2.60	1.57	0.41	0.26	0.25	0.61	0.42
5.80	2.20	1.07	0.23	0.30	0.31	0.44	0.34
			Silicon				
2.45	2.81	2.29	0.52	----	----	0.71	0.41
2.85	3.04	2.27	0.77	----	----	0.77	0.46
4.00	2.10	1.50	0.56	----	----	0.81	0.50
4.90	2.50	1.57	0.92	----	0.02	0.80	0.52
5.80	2.20	1.19	0.70	----	0.08	0.67	0.47

Cross sections are in barns. Energy is in MeV.

do not take them into account. In principle, if there were only a few charged particle groups emitted, it should be possible to obtain transmission coefficients for the emitted protons and alphas using the optical model calculations with the appropriate parameters. These could then be used in the branching ratio factor of the Hauser-Feshbach formula. Unfortunately, optical model calculations for low energy charged particles (especially alpha particles) incident on light nuclei could not be expected to give reliable transmission coefficients for describing the decay of the compound system by these channels. In this case, there is virtually a continuum of levels in ^{32}P and ^{29}S to which the compound system may decay by proton or alpha emission. Therefore, any attempt at taking these competing reactions into account was eschewed. Thus, for sulfur, the inelastic and compound elastic scattering cross sections predicted by the Hauser-Feshbach and Dresner formulas will be overestimated since these competing decay channels are not taken into account.

For both silicon and sulfur, even in the cases where $\langle \Gamma \rangle \gg D$, our results depend on a number of assumptions which may not be valid. We have ignored the possibility of any direct reactions. It is possible that there may be a small contribution from direct reactions, and moreover that the division of the transition amplitude into two parts, one approximately constant and the other rapidly varying, may not be realistic. In reality, $\mathcal{J}_{cc'}$ may be composed of terms with a continuum of frequencies.

Another important assumption is that the non-diagonal transition amplitudes are uncorrelated, i.e., that

$$\langle \gamma_{\lambda c} \gamma_{\lambda c'} \rangle = 0$$

and hence that $\langle \mathcal{J}_{cc'}^{fluct} \rangle = 0$. If this is not true, then inspection of

Eq. (32) shows that the cross section $\sigma_{cc'}$ may be increased or decreased depending on the effect of $\langle \mathcal{J}_{cc'}^{fluct} \rangle$ on the partial cross sections $\sigma_{cc'}^{corr}$ and $\sigma_{cc'}^{fluct}$. Moldauer (1964) has pointed out that the presence of such correlations will also tend to increase the magnitude of the fluctuations described by Ericson.

Another source of possible fluctuations is the presence of the "doorway states" described by Feshbach (1962). These can be differentiated from the Ericson fluctuations, however, since they should be present in different partial cross sections at the same excitation in the compound system. For example, a fluctuation due to a doorway state which appears in an inelastic scattering cross section should also appear in the compound elastic cross section at the same energy.

The most important results obtained above may be summarized as follows:

(1) We have obtained formulas for calculating elastic and inelastic differential cross sections which predict the average value of these cross sections over large energy intervals.

(2) Since the cross sections have shown large fluctuations, we cannot, in general, expect precise agreement between the theoretical calculations and the experimental measurements.

(3) We have obtained formulas which enable estimates to be made of the magnitudes and periods of these fluctuations.

(4) The validity of the formulas for describing the cross sections and their fluctuations depends on a number of stringent assumptions; the most important of which is that, at the excitation of the compound system, we must have $\langle \Gamma^{J\pi} \rangle >> D_{J\pi}$.

(5) We cannot accurately estimate the ratio $\langle \Gamma^{J\pi} \rangle / D_{J\pi}$ and it is possible that we may have $\langle \Gamma^{J\pi} \rangle \approx D_{J\pi}$, particularly at the lower bombarding energies used in the experiment.

(6) In the case of sulfur, we cannot take the competing (n,α) and (n,p) reactions into account in our calculations. Therefore, the calculated inelastic scattering cross sections for sulfur will, in general, be too large.

The reservations contained in statements (2), (4), (5), and (6) must be borne in mind when comparing the theoretical predictions to the data.

CHAPTER III

EXPERIMENTAL APPARATUS AND PROCEDURE

A. The Time-of-Flight System

Determination of the energies of neutrons by time-of-flight techniques has been facilitated in recent years by the development of fast pulse-circuitry, fast scintillators, and high-gain, low-noise photomultiplier tubes. The Duke University time-of-flight system (Lewis et al, 1959; Kapadia, 1963; Buccino, 1963; Hollandsworth, 1963) was designed for neutron spectroscopy in the MeV range of neutron energies.

In previous studies of inelastic neutron scattering using this system (Wilenzick, 1962; Buccino, 1963; Hollandsworth, 1963; Kapadia, 1963) a continuum of scattered neutron energies was observed, resulting from the excitation of the many overlapping levels in the medium and heavy-weight target nuclei used. The silicon and sulfur nuclei studied in this experiment have energy levels spaced far enough apart so that groups of scattered neutrons which have excited different levels can be resolved in the time-of-flight spectrum. This study has been facilitated by recent improvements in detector shielding and electronic circuitry which have improved the ratio of signal to background.

1. Beam Pulsing. In order to achieve the time resolution and average beam current needed for this experiment, a combination of pre- and post-acceleration beam pulsing was used. The DC beam of the Duke University 4 MV Van de Graaff accelerator is first chopped by sweeping the DC beam across a burst-defining slit in the high energy terminal of the machine. This provides neutron pulses with a duration of about 10 ns. The sweep frequency is 5 MHz and a refractor removes one of the two bursts per cycle from the beam so that the repetition rate is 5 million per second. After acceleration, these pulses are swept across a second pair of burst-defining slits which can be used to reduce the burst duration to less than 2 ns. Since the average beam current is decreased by a corresponding amount, in practice only enough external pulsing was used to provide reasonable time resolution while retaining as much average beam current as possible.

The complications involved in using two-fold pulsing are justified for the following reasons: (1) Due to size limitations, the terminal pulser cannot be made to produce bursts of duration less than about 10 ns without decreasing peak beam; (2) if external pulsing alone were used, the DC beam current required to produce usable average beam after chopping would overload the beam tube; and (3) the neutron background produced by chopping a DC beam externally would be prohibitively large when deuterons are the particles being accelerated.

A block diagram of the electronic apparatus used in the experiment including the arrangement for externally pulsing the beam is shown in Fig. 2.

After acceleration and momentum analysis, beam pulses produced in the terminal pass through a stainless steel tube (pick-up-loop) inducing voltage pulses in the tube which are nominally 1 mv in amplitude. An emitter follower with an input circuit tuned to 5 Mc/sec is attached directly to the

Figure 2. Block Diagram of Electronics

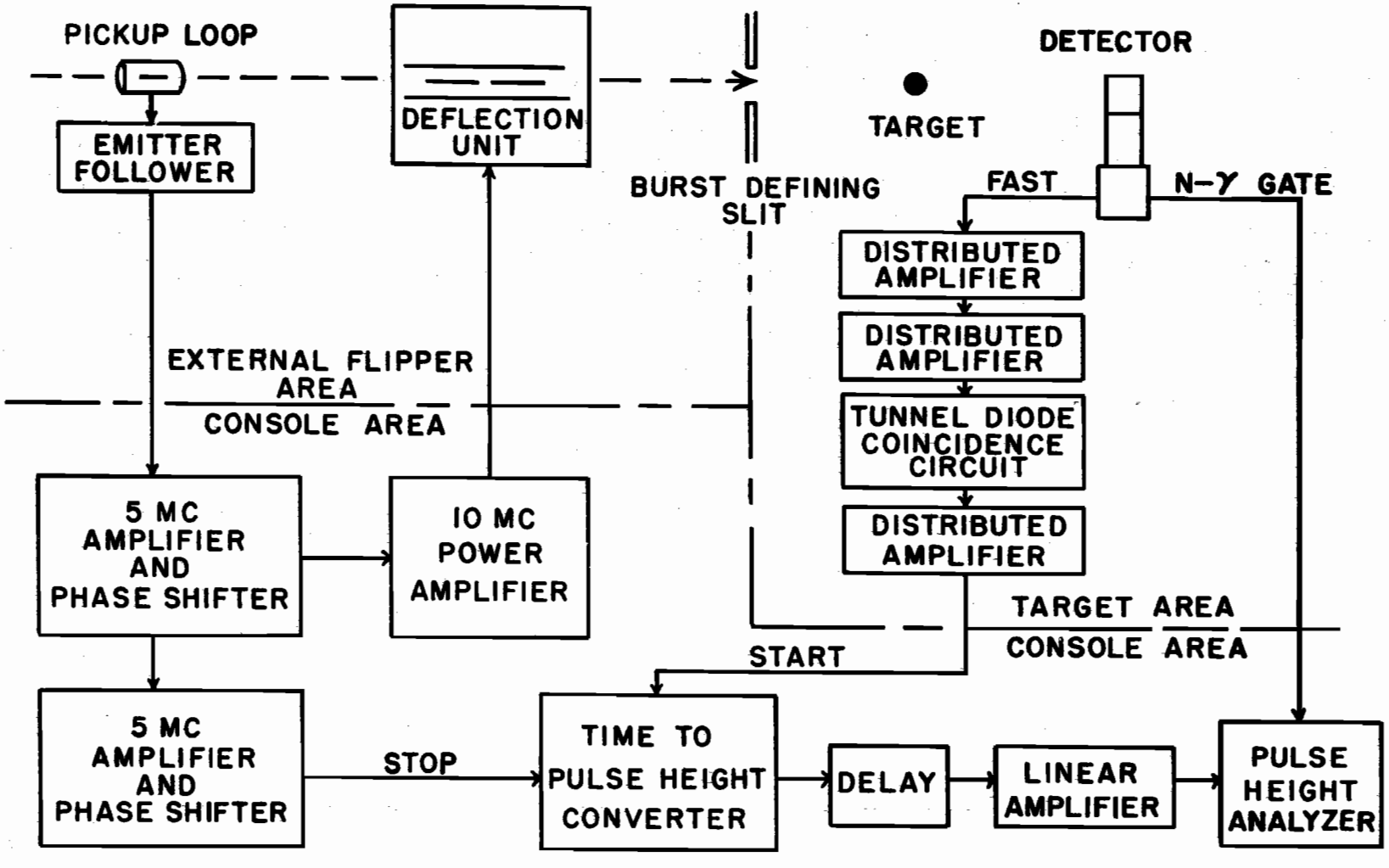
PICKUP LOOP
EMITTER FOLLOWER
DEFLECTION UNIT
BURST DEFINING SLIT
TARGET
DETECTOR
FAST
N-γ GATE
DISTRIBUTED AMPLIFIER
DISTRIBUTED AMPLIFIER
TUNNEL DIODE COINCIDENCE CIRCUIT
DISTRIBUTED AMPLIFIER
EXTERNAL FLIPPER AREA
CONSOLE AREA
5 MC AMPLIFIER AND PHASE SHIFTER
10 MC POWER AMPLIFIER
TARGET AREA
CONSOLE AREA
START
5 MC AMPLIFIER AND PHASE SHIFTER
STOP
TIME TO PULSE HEIGHT CONVERTER
DELAY
LINEAR AMPLIFIER
PULSE HEIGHT ANALYZER

pickup loop. This produces a 5 Mc/sec sine wave which is amplified by a tuned 5 Mc/sec amplifier and phase shifter. The output of this amplifier drives a 10 Mc/sec tuned power amplifier. The power amplifier was designed to resonate at 10 Mc/sec rather than 5 Mc/sec in order to reduce regenerative feedback and prevent free oscillations (Hollandsworth, 1962; Bevington, 1960; Lewis et al, 1959).

Previous to this experiment, the output of the power amplifier was capacitively coupled directly to the external deflection plates. However, the large detector shield constructed for this experiment was found to act as an antenna, picking up several harmonics (up to the eleventh harmonic) of the 10 Mc/sec voltage produced at the power amplifier output. This voltage, in turn, was picked up by the phototube base and was superimposed on the signal from the phototube. All attempts at shielding the power amplifier failed to reduce this pickup.

The problem was solved by moving the power amplifier to the accelerator console area from its original position directly underneath the beam deflection plates and transmitting power to the deflection plates through about fifteen feet of coaxial cable. A diagram of the 10 Mc/sec power amplifier showing the method used to transmit power to the deflection plates is given in Fig. 3.

Power is coupled to the coaxial cable from the tank circuits at each end of the cable by impedance matching transformers. Each transformer consists of a small loop of wire inserted into the tank circuit coil concentrically with it. This loop is connected to the cable through a uhf connector. The tank coil consists of about eight turns of wire and the loop of only two turns. This loop-within-coil acts as a transformer, matching the low impedance cable to the high impedance tank circuits.

Figure 3. Power Amplifier and Deflector Plates

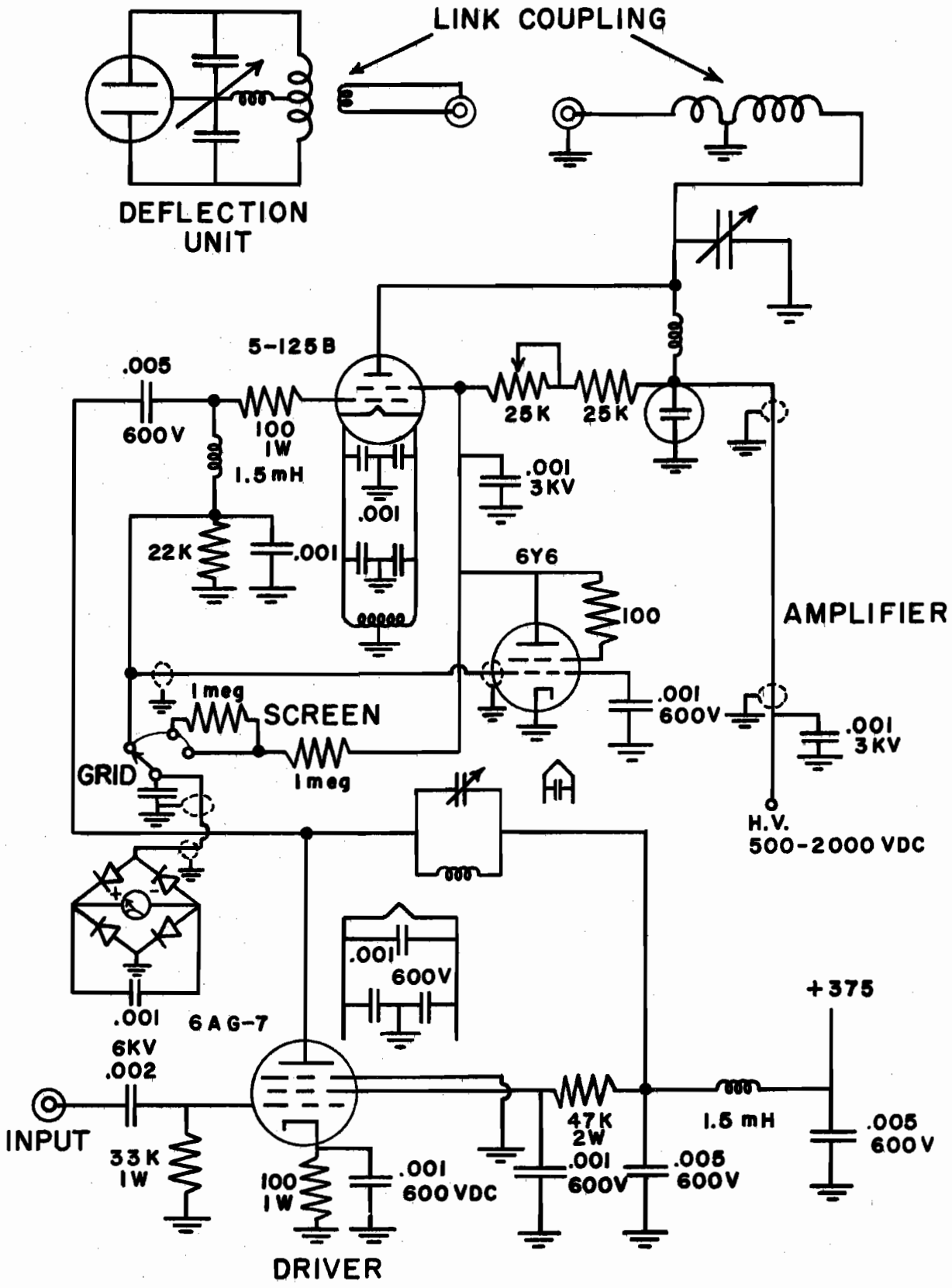
LINK COUPLING
DEFLECTION UNIT
5-125B
.005
600V
100
1W
1.5mH
22K
.001
.001
.001
3KV
25K
25K
6Y6
100
AMPLIFIER
1meg
SCREEN
1meg
GRID
.001
600V
.001
3KV
H.V.
500-2000 VDC
.001
600V
.001
6KV
.002
6AG-7
INPUT
33K
1W
100
1W
.001
600 VDC
47K
2W
.001
600V
.005
600V
1.5 mH
+375
.005
600V
DRIVER

The tank circuit adjacent to the flipper plates is mounted in a metal box which is attached to the beam tube and surrounds the flipper plates. As shown in the figure, this tank circuit is connected in parallel with the beam deflection plates. When the power amplifier is operated, both tank circuits are tuned until maximum power is transmitted to the flipper plates.

With this arrangement, the signal from the photomultiplier tube showed no indication that the water tank was picking up radiation from either the power amplifier or deflection plates. Also, the power amplifier was more accessible at the console than near the deflection plates, thus making it easier to vary the deflection voltage.

2. Neutron Sources. In order to obtain monoenergetic neutrons over a large energy range, two reactions were employed. The $T(p,n)He^3$ reaction was used to produce neutrons from threshold up to about 3 MeV and the $D(d,n)He^3$ reaction provided neutrons with energies up to 7 MeV.

A target chamber was designed and built to contain tritium gas for the T(p,n) reaction. However, due to the health hazard involved in the use of tritium gas, a solid target was finally used. Three solid tritium-zirconium targets were obtained from the Isotope Sales Division of the Oak Ridge National Laboratory. These targets are made by first evaporating a uniform layer of zirconium on a platinum backing. The target is then heated to about 400° C in an atmosphere of tritium. When allowed to cool, the metal absorbs tritium. The standard target made by ORNL contains 500 ug/cm^2 of zirconium metal with a H^3-Zr atomic ratio of 1:1. The thickness of such a target is about 50 keV for protons at threshold for the T(p,n) reaction. A standard "50 keV" target and a thinner "10 keV"

target were obtained. Since the theoretical interpretation of the data allowed a large energy spread in the incident neutron beam and since a high neutron flux was desirable, a third target, 5 times as thick as the standard target, was ordered from ORNL. Despite several attempts at fabrication, a target with a yield about three times that of the standard 50 keV target was the thickest obtainable. This target was too thick for its thickness to be accurately measured directly at threshold, but the variation of the yield with energy in conjunction with its relatively high yield indicated that it was about 200 keV thick at threshold.

The target was used in taking the angular distributions at 2.45 and 2.85 MeV, and the 50 keV and 10 keV targets were used in taking the 60° excitation curve.

A gas target chamber consisting of a cylinder 1 inch long with a nickel foil entrance window (Rolland 1963) was used in obtaining neutrons from the $D(d,n)He^3$ reaction. The thickness of the gas target was considerably larger than the solid tritium-zirconium targets. Table II lists the incident particle energy and neutron source characteristics for each of the incident neutron energies used in measuring the angular distributions. The deuteron energy loss in both the entrance window and gas chamber is included as well as the deuteron energy spread caused by inhomogeneity in the nickel foil. Tests conducted at this laboratory (Parks, 1963) have shown that this inhomogeneity is about 10% of the thickness of the foil. Straggling was not taken into account since its effect on the energy spread is negligible compared to that due to the foil inhomogeneity.

For neutron energies less than about 4 MeV, the heat dissipated by the deuteron beam in passing through the foil window of the gas target chamber becomes large enough to weaken the foil, markedly increasing the

Table II. Neutron Source Properties

Incident neutron energy E_n, deuteron (proton) bombarding energy E_0, energy loss in nickel foil E_f, and target thickness E_t.

E_n (MeV)	E_0 (MeV)	E_f (MeV)	E_t (MeV)
2.45	3.30	----	.128
2.85	3.69	----	.120
4.00	1.02	.155	.260
4.90	1.86	.114	.330
5.80	2.68	.094	.238

All calculations are for 1μ Ni foil. Two highest energies are for 2 atmospheres target pressure. One atmosphere pressure used at 4.00 MeV. Two lowest energies are for thickest H-Zr target.

danger that it will rupture. Moreover, the energy spread in the deuteron beam due to foil and target thickness results in an energy spread in the emitted neutrons which becomes prohibitively large for neutron energies below 4 MeV. The target thickness can be reduced by decreasing the gas pressure; however, this not only reduces the neutron yield but also reduces the amount of heat dissipated from the foil. Thus, an arbitrary lower limit for the gas pressure of one atmosphere was used. These factors set a lower limit of 4 MeV on the energy of neutrons produced in the $D(d,n)He^3$ reaction which could be utilized. Unfortunately, no suitable reaction exists for producing neutrons with energies between three and four MeV for use in this experiment. For neutron energies above 5 MeV, the gas pressure in the gas target chamber was increased to two atmospheres without seriously impairing the energy resolution.

The accelerator voltage was measured with a precision digital voltmeter used in conjunction with a precision AC-DC converter and the original generating voltmeter of the accelerator (Hollandsworth et al, 1964). This system was calibrated frequently using the threshold of the $Li^7(p,n)Be^7$ reaction as the calibration point. The linearity of the system has been checked by comparing the digital voltmeter reading with the beam energy indicated by an electrostatic analyzer over an energy range of from one to four MeV. The indicated voltage at the Li(p,n) threshold has been found to be reproducible to within about 4 keV over a period of several days.

During the measurement of the 60° excitation curves, the machine voltage was calibrated by measuring the energy of the resonance in carbon at 2.1 MeV neutron energy. As expected, the voltage reading at this point was reproducible to within about 10 keV over a period of several days.

3. Neutron Detection System. A Nuclear Enterprises, Ltd. Pulse Shape Discrimination (PSD) Probe, model NE5571, was used as the neutron detector. It utilizes a type NE213 liquid scintillator encapsulated in a glass cylinder two inches long and two inches in diameter mounted on an RCA 6810-A photomultiplier tube. This probe was specially constructed with a "fast" output taken from a 200 ohm load on the 14th dynode as well as the standard "linear" output taken from dynode 11 and PSD output from the anode and dynode 13.

The linear output was not used in this experiment. Instead, start pulses for the time-to-pulse-height coverter were derived from the fast signal, and the PSD output was used to gate the input of the pulse height analyzer. The time-to-pulse-height converter is of Los Alamos design (Weber et al, 1956).

Photomultiplier tube pulses which arise from a gamma ray incident on the scintillator can be differentiated from pulses produced by incident neutrons because the overall shapes of the two kinds of pulses are quite different. This provides a way to discriminate against the unwanted gamma ray pulses. Discrimination is achieved by making use of the fact that the ratio of the slow to fast components of phototube pulses is greater by about a factor of two for pulses produced by protons than for electron pulses. The PSD circuit is based on the design of Brooks (1959), but uses simpler and faster circuitry designed by Daehnick and Sherr (1961).

A negative signal proportional to the fast component is obtained by differentiation of the anode current pulse with a very short time constant (approximately 10 nsec). The negative part of this pulse is then shaped and stretched so that its duration is approximately the same as the slow component from dynode 13. Meanwhile, the leading negative spike from the anode is used to short the fast portion of the positive pulse from the 13th dynode to ground. The remaining slow portion of the pulse is stretched and added to the fast

pulse from the anode. The circuit parameters are adjusted so that fast and slow pulses due to an electron cancel each other whereas the pulses due to a heavy particle produce a net positive output. After amplification by a non-overload amplifier, the pulses pass through a discriminator. The output pulses from the discriminator are shaped into negative square pulses by a univibrator. All of the above circuitry forms a part of the base of the NE5571 PSD probe. The negative pulses from the univibrator are inverted and used to gate the multichannel analyzer.

In order to reduce the number of noise pulses reaching the converter and at the same time avoid the large amount of time-jitter that would be introduced by using a simple discriminator, a dual-channel coincidence circuit (Buccino et al, 1964) was used to reduce photomultiplier tube noise and produce signal pulses for the converter that are relatively free from time-jitter. A block diagram of this circuit is shown in Fig. 4.

The fast signal from the photomultiplier tube is first amplified by two wide band amplifiers. In the coincidence circuit, the signal is first split into two channels, each of which contains a tunnel diode discriminator. The tunnel diode in the "fast" channel is biased to trigger on very small pulses. Thus, it triggers on the first part of the pulses, and its output is relatively free from time-jitter. However, it triggers on many phototube noise pulses as well as on the desired signal pulses. The tunnel diode in the "slow" channel is biased to trigger only on large pulses, thus rejecting most of the noise pulses from the phototube. This is done at the cost of introducing a large amount of time-jitter in this channel. The pulses in both channels pass through a second set of tunnel diode univibrators in which the "slow" pulse is shaped and stretched and the fast pulse is shaped and then delayed with 12 feet of RG 114/U 200 ohm

Figure 4. Tunnel Diode Coincidence Circuit

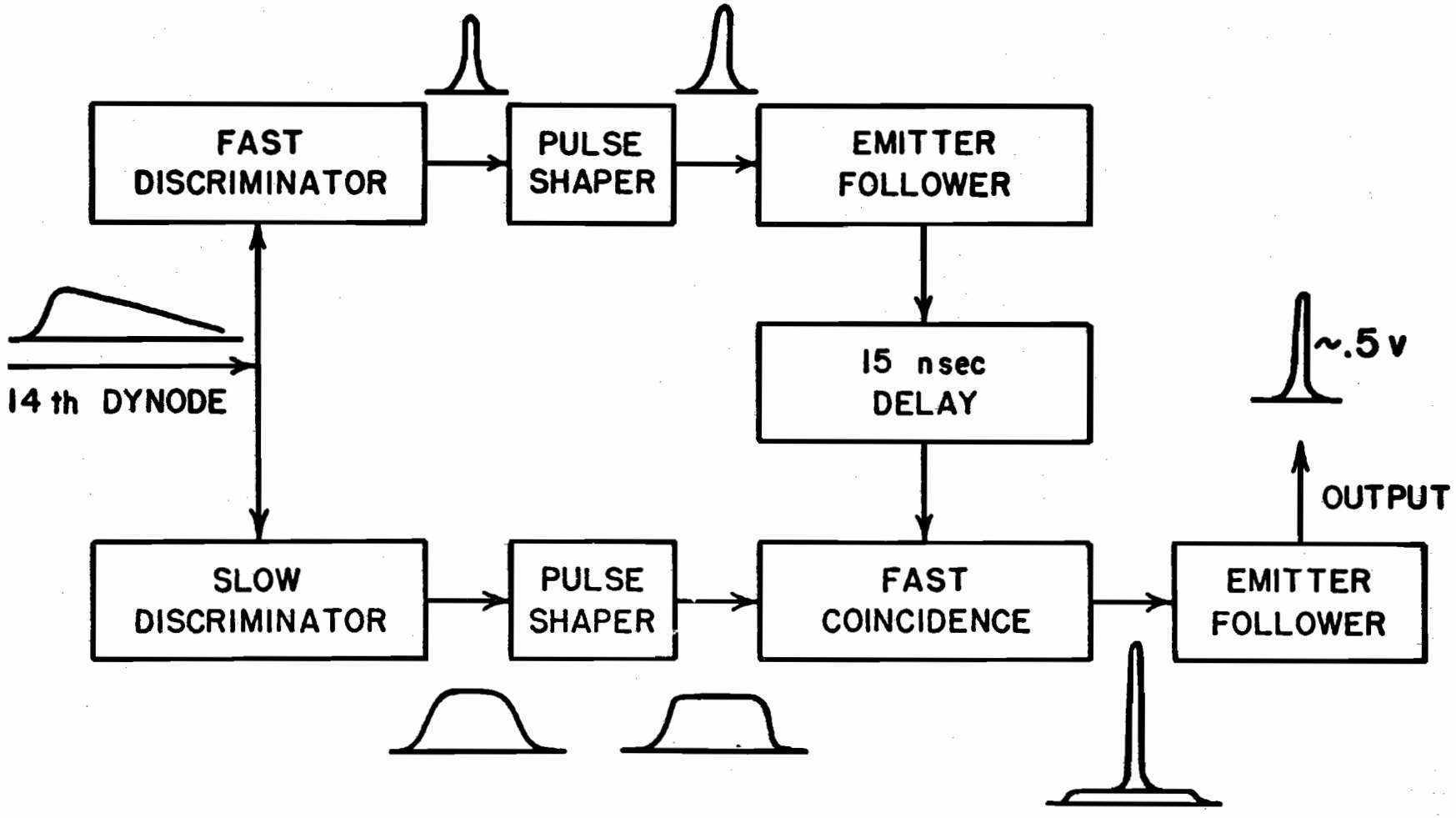

TUNNEL DIODE TRIGGER CIRCUIT

coaxial cable. In the last stage of the circuit, pulses from the two channels are added at a tunnel diode which is biased to trigger only when signals from both channels appear in coincidence. Since the fast signal is delayed, the long duration pulse in the slow channel arrives at the coincidence input first, and the coincidence tunnel diode triggers when the fast pulse arrives. Thus, the circuit discriminates against noise pulses and at the same time retains the timing properties of a discriminator set low enough to trigger on the leading edge of the phototube pulses.

The output of the trigger coincidence circuit is then amplified and inverted in a wide band amplifier to form the "start" pulse for the time-to-pulse height converter. The output pulses from the converter are next amplified by a non-overload amplifier and connected to a 400 channel pulse-height analyzer for analysis.

4. Detector Efficiency. The data points in each angular distribution must be adjusted relative to each other to compensate for the variation of detection efficiency as the scattered neutron energy decreases with increasing scattering angle. Moreover, the data for the inelastically scattered neutrons must be adjusted relative to those of the elastically scattered neutrons to compensate for the different detector efficiency at the lower neutron energy.

The efficiency of the detector relative to that of the long counter was determined by comparing the observed yield of the neutron source as a function of neutron energy as determined by the detector and by the long counter, located symmetrically about 0°.

It has been found that the measured efficiency is affected by the choice of angle. In particular, at 60° the measured efficiency drops

unrealistically fast with increasing neutron energy above about 1 MeV. This has been ascribed to the following: The shape of the angular distribution of neutrons from the T(p,n) reaction changes drastically as the incident proton energy increases and a sharp minimum begins to appear at 60° as the incident proton energy increases above about 1 MeV. The long counter subtends a much larger solid angle than the detector; therefore, if both detector and counter are placed at 60°, the detector will see only a neutron flux proportional to the yield at the minimum in the angular distribution, whereas the long counter will see a flux proportional to the yield averaged over a comparatively large angular range about the minimum. As the minimum becomes sharper with increasing energy, the detector sees an increasingly smaller flux relative to the long counter and the efficiency calculated from these measurements drops correspondingly.

This effect can be minimized by using an angle of less than 45°. An angle of 30° was used for all efficiency measurements made during this experiment. This permitted measurement of the detector efficiency from threshold up to an energy of about 2.8 MeV.

The efficiency curve for a detector with an organic scintillator is expected to follow the theoretical n-p cross section and can be approximated provided the effective energy threshold for detection is known (Bevington, 1960). Accordingly, the experimentally determined threshold (250 keV) was used to calculate theoretical points covering the higher energy range.

In order to obtain an experimental check on these calculations for energies higher than 2.8 MeV, the long counter was placed on the gun-mount turntable at 90° with respect to the detector. By rotating the gun-mount so that the detector and long counter were alternately at 90°

and 0° to the direction of the incident beam, the efficiency could be measured for two different neutron energies without changing the incident particle energy. The $D(d,n)He^3$ reaction was used to produce neutrons in the energy range from 2.6 to 3.1 MeV at 90° and 4.0 to 5.8 MeV at 0°. The efficiency curve measured in this way is subject to large errors because of the large neutron background which is always present and which varies rapidly with machine energy when deuterons are accelerated. This background is seen by the long counter to a far greater extent than by the detector, and there is no way to correct for this discrepancy. More errors are introduced by the necessity for normalizing the 90° data to the 0° data and then normalizing both of these to the lower energy measurements made using the $T(p,n)He^3$ reaction.

Despite these large errors, the measured curve in this energy range agreed well with the calculated curve. Thus, there is no experimental evidence to indicate that the calculated curve is not an accurate way to determine the detector efficiency.

B. Choice of Experimental Parameters

The nuclei studied in this experiment were chosen not only because of their interest from a theoretical standpoint, but also because of the capabilities and limitations of the time-of-flight system.

From a theoretical standpoint, it is interesting to test the predictions of the statistical model in the case where the residual target nuclei have a discrete number of excited levels. The limitations of the time-of-flight system require that these final excited states be widely spaced. This restriction is necessitated by the time resolution that can

be achieved with the neutron energies, flight paths, and beam pulse durations available with the system.

The relationship between neutron flight time and neutron energy is given by $T = \frac{72.3}{E} L$ where T is in ns., E is in MeV and the flight path, L, is in meters. From this expression, it can be seen that the separation in time between two neutrons scattered from a nucleus with different energies decreases with increasing incident neutron energy.

Using the $D(d,n)He^3$ reaction, the Duke University 4 MV accelerator can be used to produce neutrons with energies up to about 7 MeV. If this high an energy is used, neutron groups scattered with different energies can be resolved in time only if a long flight path is used and if the time duration of the beam pulses is made very short. However, in order to obtain a reasonable neutron flux, the beam pulse duration could not be reduced below about 5 ns. The scattered neutron flux decreases with the square of the flight path while the neutron background has been found to be fairly independent of this distance. Therefore, the flight path cannot be increased beyond about 1.5 meters before the ratio of background to signal becomes prohibitively large.

These considerations suggested that light-weight nuclei with widely spaced levels be studied. Since the results of the experiment were to be compared with the predictions of the optical model and the statistical model, the target nuclei had to be heavy enough for these comparisons to be valid. This dictated that nuclei with $A \approx 20$ be used. In this mass range, studies similar to this experiment had already been performed on Mg^{24} (Thomson, 1962), Na^{23} (Towle and Gilboy, 1962), and Al^{27} (Towle and Gilboy, 1962).

Two nuclei in the same nuclear mass range which had not been studied were silicon and sulfur. Unlike the nuclei already studied, they are both

even-even nuclei and consequently have very high first excited states. Fig. 5 shows level diagrams for these nuclei. Thus, by using a flight path of 1.5 meters, scattered neutron peaks resulting from excitation of the first excited states in these nuclei could be fairly well resolved in the time-of-flight spectrum at the highest incident energies obtainable with the Duke University accelerator.

A brief survey revealed that even at the highest obtainable energy the second and higher excited states in both silicon and sulfur were only slightly excited so that the peaks in the time-of-flight spectra due to scattered neutrons which left the residual nuclei in these states could not be separated from background. Therefore, the maximum incident energy at which angular distributions were taken was 5.8 MeV. At this energy, by using a flight path of 1.5 meters, the peak due to elastically scattered neutrons and the peak due to neutrons which left the residual nucleus in its first excited state could be resolved even at a scattering angle of 30° where the elastic peak was several times as large as the inelastic peak. The time-of-flight spectrum of neutrons scattered from sulfur for an incident neutron energy of 5.8 MeV is shown in Fig. 6. The small peaks resulting from the excitation of the second, third, and fourth excited states in sulfur are labeled (n_2), (n_3), and (n_4), respectively. As can be seen in the figure, the elastic peak, (n_0), is completely resolved from the peak due to neutrons which have left the residual nucleus in its first excited state, (n_1).

At incident neutron energies below about 5 MeV, the two peaks were still separated in the time-of-flight spectrum with the flight path shortened to 1.25 meters. Thus, in order to increase the counting rate, this shorter flight path was used for taking the data for incident neutron energies below 5 MeV.

Figure 5. Energy Level Diagrams for Silicon and Sulfur

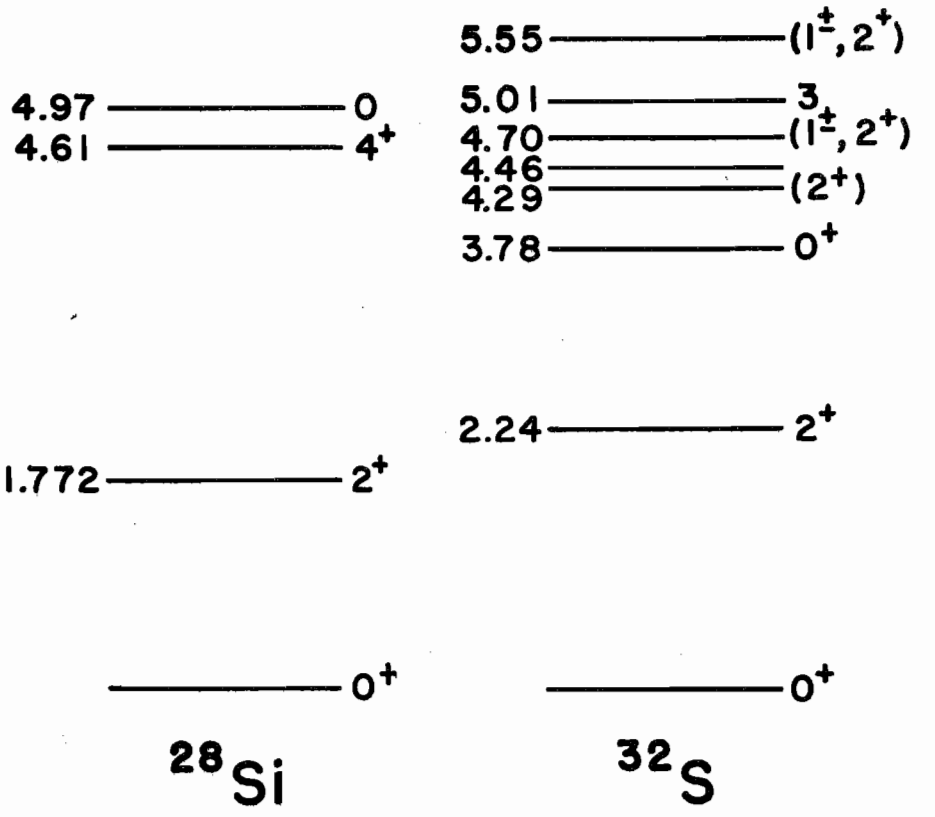
5.55
(1±, 2+)
5.01
3
4.97
0
4.70
(1±, 2+)
4.61
4+
4.46
4.29
(2+)
3.78
0+
2.24
2+
1.772
2+
0+
0+
28Si
32S

Figure 6. Time-of-Flight Spectrum of Neutrons Scattered by Sulfur

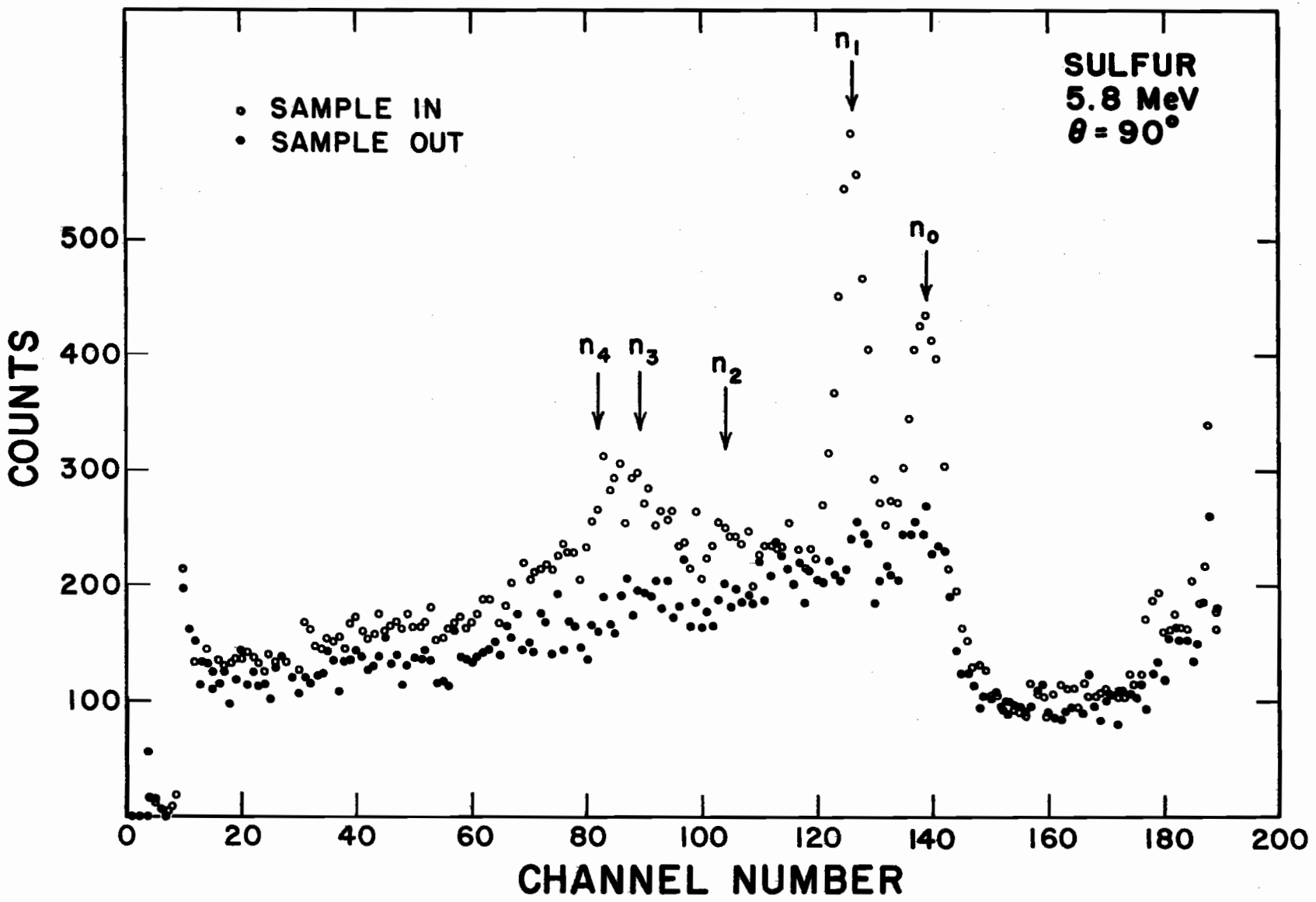
SULFUR
5.8 MeV
θ = 90°
SAMPLE IN
SAMPLE OUT
n1
n0
n2
n3
n4
COUNTS
CHANNEL NUMBER
0
20
40
60
80
100
120
140
160
180
200
100
200
300
400
500

The level of the neutron-gamma discriminator effectively determines the bias on the photomultiplier tube. With this discriminator set to obtain a reasonable compromise between neutron counting rate and gamma-ray discrimination, the detection efficiency drops rapidly from the end of its flat portion at about 500 keV to cutoff at 250 keV (Fig. 7). This determines the lowest neutron energies at which data can be taken.

In order to determine optimum energies at which to measure angular distributions, excitation curves were measured with the detector positioned at an angle of 60°. Pronounced maxima in the excitation of the first excited state of silicon were found at 2.45 and 2.85 MeV incident neutron energy. These energies were then chosen for the two lowest energy angular distributions in order to take advantage of the relatively high counting rate for neutrons scattered inelastically by silicon at these energies. The amount of inelastic scattering from sulfur was so small that the inelastic peaks could not be extracted from the time-of-flight spectra over this whole energy range.

There were no large fluctuations in the inelastic excitation curves for either silicon or sulfur measured from 4 to 7 MeV incident neutron energy. Thus, 4, 4.9, and 5.8 MeV were chosen for the higher energy angular distributions simply because they were equally spaced over the energy range of interest.

Due to the difficulty of shielding the detector from the source at forward angles, the smallest scattering angle used was 30°. Data were taken at 15° intervals in the lab system. At the shorter flight path which was used for incident neutron energies below 5 MeV, the detector could not be rotated to an angle greater than 145°. Thus, the laboratory angles used were 30°, 45°, 60°, 75°, 90°, 105°, 120°, 135°, and 145°, except for the angular distributions measured at 4.9 and 5.8 MeV in which case a maximum angle of 150° could be used instead of 145°.

Figure 7. Relative Detector Efficiency

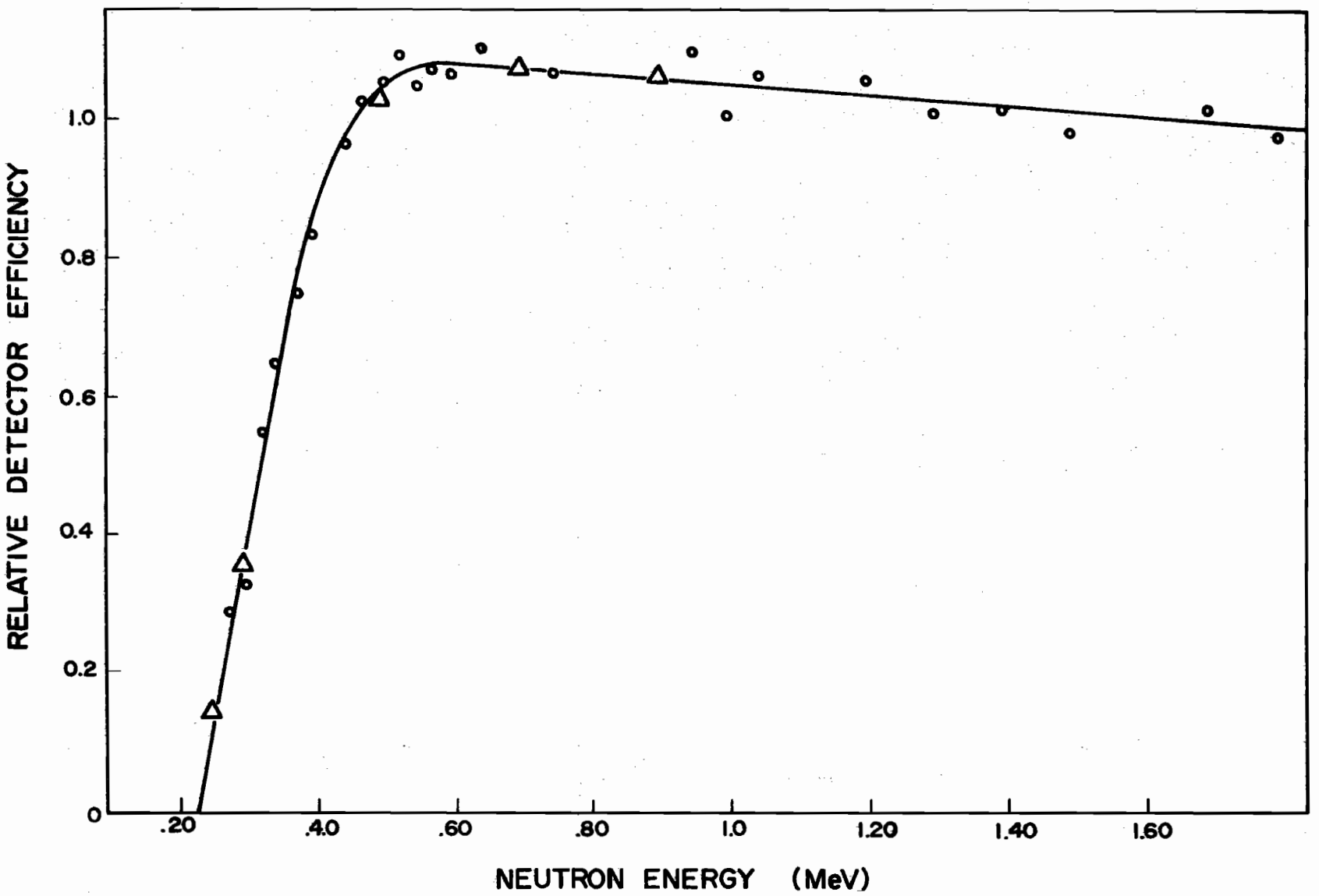
RELATIVE DETECTOR EFFICIENCY
0
0.2
0.4
0.6
0.8
1.0
.20
.40
.60
.80
1.0
1.20
1.40
1.60
NEUTRON ENERGY (MeV)

CHAPTER IV

DATA ANALYSIS

A. Angular Distribution Data Reduction

The data taken at each angle consisted of "sample-in" spectra for silicon, sulfur, and carbon, and "sample-out" spectra taken with the samples replaced by an empty can identical to the sample containers. Where time permitted, data were taken until a total of about a thousand counts above background had accumulated in the inelastic peak. This sometimes required as much as forty-five minutes per spectrum.

A computer code was used to subtract the sample-out from the sample-in data and smooth the resulting spectra. These were plotted and the areas in the peaks were measured by hand. At the higher energies, the elastic and inelastic peaks were not completely resolved. The area of each peak could be determined under these circumstances if the shape of the elastic peak was known. Unfortunately, the shape of the carbon elastic peak could not be used to determine the silicon and sulfur peak shapes because the carbon peaks had comparatively large low-energy tails which the silicon and sulfur peaks lacked. The presence of these tails is attributed to multiply scattered neutrons which have a large energy spread due to the large recoil energy of the light carbon nuclei. In order to overcome this difficulty, the areas of the peaks at all energies were measured by extrapolating the sides of the peaks straight to the base-line.

The next step in the analysis was to obtain angular distributions. The number of elastically scattered neutrons at each angle was divided by the corresponding numbers of monitor counts. These ratios were then corrected for the variation in detection efficiency with scattering angle.

The shape and magnitude of this curve were then corrected for the effects of multiple scattering and beam attenuation in the scattering sample using a computer code, MANIAC 6, a revised version of MANIAC 5 (Bevington et al, 1964). A description of the program is given in Appendix I. The program uses a Monte Carlo technique to simulate neutron scattering in the sample in the following manner: Given an elastic scattering angular distribution that is free of the effects of multiple scattering, the program analyzes the "histories" of several thousand neutrons which are scattered by a hypothetical scattering sample with the same dimensions and density as the scattering sample used in the laboratory. The resulting angular distribution which is the output of the program then closely approximates which would be measured in the laboratory. Thus, an iterative procedure may be used to obtain the angular distribution free of the effects of multiple scattering and attenuation. The measured angular distribution is used as the first input. A second input can be determined by comparing the first input and output. This is continued until an input angular distribution is obtained such that the output of the program is similar to the measured angular distribution. The distribution so obtained is then presumed to be the angular distribution that would be measured in the absence of multiple scattering, geometrical effects, and attenuation.

In the case of carbon, the angular distribution inputs are in arbitrary units. The program then integrates this angular distribution and normalizes the result to the known total elastic cross section (BNL 325).

The program then yields the "observed" angular distribution in absolute units. The normalization for the differential cross sections for the silicon and sulfur samples can be obtained from the carbon differential cross sections. The number of detector counts at a given angle is given by

$$Cts = K \times Mon \times eff \times (\#\ of\ nuclei\ in\ scatterer) \times \frac{d\sigma}{d\Omega} \tag{57}$$

where $\frac{d\sigma}{d\Omega}$ is the "observed" differential cross section, Mon is the number of neutrons detected by the Hansen-Mckibben long counter and eff is the detection efficiency of the detector relative to that at 0°. We may also write this as

$$Cts = K' \times Mon \times eff \times W/MW \tag{58}$$

where W is the weight of the scattering sample and MW is the molecular weight of the scatterer. Thus

$$\frac{d\sigma}{d\Omega} = \left(\frac{Cts}{Mon}\right) \times \frac{1}{eff} \times \frac{MW}{W} \times \frac{1}{K'} \tag{59}$$

The value of K' is determined by normalizing the carbon angular distribution to the total elastic cross section

$$\frac{1}{K'} = \left[\left(\frac{Cts}{Mon}\right)^{-1} \times \frac{d\sigma}{d\Omega} \times eff \times \frac{W}{MW}\right]_{CARBON} \tag{60}$$

Thus, equations (54) and (55) give an "observed" cross section in mb/sr.

This angular distribution is then corrected for multiple scattering, beam attenuation, and geometrical effects using the Monte Carlo computer code.

Instead of using equations (59) and (60) to obtain the silicon and sulfur cross sections, the elastic and inelastic scattering angular distributions could, in principle, be normalized to the total cross section as was done for carbon. In practice this is impractical for several reasons: (1) The only previously measured cross sections for silicon and sulfur are the total cross section and the (n,p) and (n,α) partial cross sections. The magnitudes of these partial cross sections are appreciable at all the bombarding energies used in the case of sulfur and they also exhibit large, rapid fluctuations with energy. They would have to be subtracted from the total cross section to obtain the neutron scattering cross section and the uncertainty introduced by this procedure would be very large. (2) The total cross sections of both nuclei fluctuate rapidly and strongly with energy, making exact determination of the total cross section at a given bombarding energy difficult. (3) The inelastic scattering cross sections for excitation of the higher excited states could not be accurately measured in this experiment, and thus could not be subtracted from the total cross section.

However, the cross sections determined for silicon and sulfur using Eq. (59) are in good agreement with previously measured values for the total cross sections (BNL 325) in the cases where the scattering cross sections measured in this experiment could be added to the (n,p) and (n,α) cross sections measured in other experiments (BNL 325).

B. Sources of Error

The purely statistical errors resulting from the fluctuations in the peak and background counts vary from a completely negligible error in the large, forward angle elastic peaks to a maximum of about $\pm$ 7% in the worst

cases for the inelastic peaks. Typically, however, the statistical errors in the inelastic peaks were about $\pm$ 4%. This also was the case for the elastic peaks at the minima and at back angles. Errors for the carbon elastic peaks were about half these values. Errors also resulted from the difficulty in deciding, in the case of the inelastic peaks, just what to include in the peaks. The sample-in background was consistently slightly higher than the sample-out background in the region between the elastic and inelastic peaks and for ten to twenty channels beyond the inelastic peak. This was presumably due to the tail of the elastic peak and, in the case of silicon, to excitation of levels in other isotopes in the sample. Besides Si^{28}, silicon has two isotopes, Si^{29} and Si^{30}, whose isotopic abundances are 4.7% and 3.1% respectively. The two of these combined have many levels in the region from zero up to 2.3 MeV. At 2.45 and 2.85 MeV incident energy, one state is excited in Si^{29} which gives an inelastic peak midway between the elastic peak and the Si^{28} inelastic peak. This peak was not discernible above the uniform background. At the higher energies, more levels in Si^{29} and Si^{30} are excited which should provide a fairly uniform background underneath the Si^{28} inelastic peak. Inspection of the time-of-flight spectra shows that this was apparently the case. Therefore, a small extra background subtraction was made by eye underneath the inelastic Si^{28} peaks in order to account for both the tail on the elastic peak and the inelastic peaks due to scattering from excited states in the other isotopes. In the case of sulfur, there is only one other isotope, S^{34}, which has a significantly large abundance; and it has only one level which would interfere with the interpretation of the S^{32} data. The energy of this level is such that the resulting peak in the time-of-flight spectrum always falls directly underneath the S^{32} inelastic peak. Therefore, its existence was simply ignored in the analysis of the data as though sulfur

were isotopically pure S^{32}. Whenever necessary, however, a small extra background subtraction was made to remove the contribution to the inelastic peak from the tail on the elastic peak.

It was by no means clear just how much of the extra background that was subtracted from the inelastic peaks belonged to the elastic tail and inelastic peaks from other isotopes and how much of it actually belonged to the inelastic peak itself. The presence of this background also made it difficult to judge how to extrapolate the sides of small inelastic peaks to the baseline. These uncertainties typically resulted in an error in determining the inelastic peak area of about $\pm$ 5%. Thus, typical relative errors in the data points in each inelastic scattering angular distribution are about $\pm$ 7%. However, at the forward angles at 4.9 and 5.8 MeV, the elastic peaks so swamped the inelastic peaks that much larger errors resulted from separating the inelastic from the elastic peaks. The worst case was silicon at 30° scattering angle and at 5.8 MeV bombarding energy where the uncertainty in separating the inelastic from the elastic peak is about $\pm$ 20%. There were other sources of error in determining the angle integrated differential cross sections. First, the carbon cross sections to which the data were normalized are known only to within about $\pm$ 5%. Another uncertainty of about $\pm$ 5% results from the uncertainty in extrapolating the carbon angular distributions to 0° and 180° which introduces the same error into the ratio $\left(\frac{\text{Cts}}{\text{Mon}}\right)^{-1}$ of Eq. (60). The same error is present in extrapolating the silicon and sulfur elastic scattering angular distributions. The remaining errors are: (1) An uncertainty of about $\pm$ 2% due to the relative uncertainties of the data points described above. (2) An uncertainty in the weight of the samples of about $\pm$ 2%. (3) An uncertainty in the correction for multiple scattering, beam attenuation, and geometrical effects of about $\pm$ 3%. Thus, the typical total uncertainty

in the determination of the silicon and sulfur elastic cross sections is about ± 10%.

The inelastic angular distributions, being nearly isotropic, could be extrapolated to 0° and 180° with little uncertainty. However, the integrated inelastic cross sections were subject to other uncertainties which were not present in the elastic angular distributions: (1) The uncertainty in the correction for multiple scattering and beam attenuation is larger in the case of inelastic scattering than elastic scattering and introduces an error that is estimated to be about ± 5%. (2) An uncertainty of about ± 4% is introduced in measuring the relative detection efficiency at the energy of the inelastically scattered particles. (3) A consistent error of about ± 5% should be allowed for the uncertainty in subtracting the "extra" background due to the tail on the elastic peak and the presence of the inelastic scattering peaks from the other isotopes. Thus, the inelastic scattering cross sections are, in general, known to within about ± 12%.

C. Excitation Curve Data Reduction

The analysis of the data for the excitation curves was somewhat different from that for the angular distributions. As in the case of the angular distributions, sample-in spectra for silicon and carbon and a sample-out spectrum were taken at every energy for which the excitation curves were measured. Data were taken for sulfur only at energies higher than 4 MeV where the inelastic scattering peak could be extracted from the spectrum. The cross section scale for the silicon and sulfur excitation curves was not obtained by normalization to the carbon cross section. Instead, a cross

section scale in arbitrary units was obtained for carbon, silicon, and sulfur individually using the following formula:

$$\frac{d\sigma'}{d\Omega} = \left(\frac{Cts}{Mon}\right)\left(eff(E')\right)^{-1}\left(\frac{I_{MON}}{I_S}\right)_E \qquad (61)$$

where E' is the energy of the scattered neutrons, $eff(E)$ the relative efficiency for detection of neutrons of energy E and I_{MON} and I_S are the neutron fluxes emitted from the neutron source in the direction of the monitor and scattering sample respectively. No corrections were made for multiple scattering or attenuation in the scattering sample. The excitation curves obtained using this formula were then normalized to the cross section values obtained from the angular distributions at 4.0, 4.9, and 5.8 MeV.

The consistency of the data above 4 MeV is gratifying in light of the fact that it depends on the ratio $\frac{I_{MON}}{I_S}$ which was not measured during the experiment but was taken from a compilation of measurements of other workers (Fowler and Brolley, 1956). The measured detector efficiency shows small fluctuations in this energy region, apparently because the long counter detects a neutron background which fluctuates with energy. This would also cause the ratio $\frac{Cts}{Mon}$ and consequently the measured differential cross section to fluctuate with energy. The consistent agreement between the differential cross sections obtained using Eq. (61) and the differential cross sections obtained from the angular distribution measurements using Eq. (59) are further evidence that these fluctuations are small. Moreover, it indicates that the long counter is not affected by a monotonic increase with energy of neutron background from spurious reactions.

D. Theoretical Comparisons

The angular distributions and excitation curves were compared with the predictions of the optical model and the theory of Hauser and Feshbach using the computer code ABACUS II (Auerbach, 1962). This code has provisions for making calculations with a number of different well shapes. In addition, provision can be made to use the non-local potential of Perey and Buck (Bevington, 1964).

Three potential types were used in the calculations. These were the potential of Bjorklund and Fernbach (1958), the non-local potential of Perey-Buck and their equivalent local potential (1962). All three employ local spin-orbit potentials of the Thomas type

$$V_{so} = -V_{sr}\,\frac{1}{r}\left|\frac{d}{dr}V_{re}(r)\right|\vec{l}\cdot\vec{\sigma}\left(\hbar/m_{\pi}c\right)^2 \qquad (62)$$

The local potential of Perey-Buck employs the Saxon form for the real potential, and for the imaginary term it employs the derivative of the Saxon form with the same radius but a different rounding parameter.

$$V = V_{RE}\left(1+\exp(r-R)/a\right)^{-1} - V_{IM}\cdot 4a\left|\frac{d}{dr}\left(1+\exp(r-R)/b\right)^{-1}\right| \qquad (63)$$

The Bjorklund-Fernbach potential employs the Saxon form for the real potential and a guassian imaginary potential centered at the surface of the real potential

$$V = -V_{RE}/\left(1+\exp\left((r-R)/a\right) - V_{IM}\exp\left[-\left((r-R)/b\right)^2\right]\right. \qquad (64)$$

The form used for the non-local potential in Eq. (10) is similar to those

employed in the local potential model calculations. Defining $\rho = (|\vec{r}+\vec{r}'|)/2$, we have

$$-U(\rho) = [V_{RE}] f_s(\rho) + i V_{IM} f_D(\rho) \tag{65}$$

where f_S has the Saxon-Woods form

$$f_S(\rho) = [1 + \exp(\frac{\rho - R}{a})]^{-1} \qquad R = r_o A^{1/3} \tag{66}$$

and f_D gives a surface absorption term of the Saxon derivative type

$$f_D(\rho) = 4 \exp(\frac{\rho - R}{b}) [1 + \exp(\frac{\rho - R}{b})]^{-2} \tag{67}$$

For the spin-orbit function

$$V_{re}(r) = f_s(r)$$

With the exception of the well depths used in the local potential calculations, the values of the parameters used in the calculations were the same as those determined by Perey and Buck by fitting elastic scattering data for lead at 7.0 and 14.0 MeV and by Bjorklund and Fernbach by fitting neutron scattering data on several elements at 4.7 and 14 MeV. All three sets of parameters have been quite successful in fitting angular distributions over a wide range of atomic mass and bombarding energy. The values of these parameters are given in Table III.

Due to the large fluctuations observed in the cross sections, the angular distributions were not expected to agree exactly with the optical model predictions. However, there is one persistent disagreement between the predicted and measured angular distributions which is most ~~pronouced~~ pronounced at the lowest energy. In general, the measured angular distributions do not

Table III. Optical Model Parameters

Parameters used in calculations with Perey-Buck non-local (PBNL), Perey-Buck local (PBL), and Bjorklund-Fernbach (BF) potentials.

	V_{RE} (MeV)	r_0 (fm)	a (fm)	V_{IM} (MeV)	b (fm)	V_{SO} (MeV)	β (fm) ~~(MeV)~~
PBNL	71	1.22	0.65	15	0.47	7.0	0.85
PBL	See below	1.25	0.65	See below	0.47	6.2	----
BF		1.25	0.65		0.98	9.5	----

The following well depths are functions of incident neutron energy (in MeV) as follows:

PBL

$$V_{RE} = 52.5 + 1.4*E + .053*E^2$$
$$V_{IM} = 4.0 + .367*E$$

BF

$$V_{RE} = 60.2 - 3.05*E + .135*E^2$$
$$V_{IM} = 1.58 + 1.59*E - .654*E^2$$

rise as steeply from about 75° to 0° as do the optical model predictions. The question therefore arose as to whether any of the model parameters might reasonably be varied in order to achieve a better overall fit. Hofstadter (1956) has found that to within a few per cent for nuclei with $A \geq 12$, the radius at which nuclear density falls to half its maximum value at the center of the nucleus varies as $r = r_0 A^{1/3}$ and the "skin thickness", defined as the distance in which the density falls from 90% to 10% of its maximum value remains constant. This suggests that the analogous non-local potential optical model parameters, the well radius and diffuseness, should not be varied. However, Hofstadter has also found that if the nucleons are assumed to be distributed uniformly throughout the volume of the nucleus, then this "equivalent uniform density" of nucleons increases slowly with increasing A up to $A \approx 40$. Since the strength of the optical potential depends directly on the density of nuclear matter, this suggested that a corresponding decrease in potential well depth might be reasonable for nuclei as light as silicon and sulfur. Therefore, the angular distributions were calculated using the non-local potential with all well depths reduced by 10% from the values used by Perey-Buck.

Calculations of the angular distributions of elastically scattered neutrons were made using ABACUS II which has provision for using the transmission coefficients from the optical model calculations in the Hauser-Feshbach formula. Calculations were also made of the inelastic scattering cross sections corrected by the width fluctuation correct factor, Eq. (32). This was done using a computer code (Tucker et al, 1964) which uses Dresner's original formula (Dresner, 1957). This program had no provision for calculating the angular distributions of the inelastic scattering, but in view of the lack of precise agreement between experiment and theory, this was not a

significant handicap. The transmission coefficients obtained from the calculations of ABACUS II, using the non-local potential of Perey-Buck, were used in this program. Since, in general, the existence of a spin-orbit force is assumed in making optical model calcuations with ABACUS II, the transmission coefficients it calculates are of the form T_ℓ^+ and T_ℓ^-, Eq. (15). The Tucker program is only equipped to use transmission coefficients of the form $T_\ell(E)$, Eq. (7). It is interesting to note that transmission coefficients obtained from these calculations by ABACUS II using the formula

$$T_\ell(E) = \frac{\ell T_\ell^- + (\ell+1) T_\ell^+}{2\ell+1}$$

when used in the Tucker program gave Hauser-Feshbach cross sections that differed from those calculated by ABACUS II by only about 3% at most.

Another computer code was written to make calculations of the mean square fluctuations of the total cross section and to compound elastic and inelastic cross sections using equations (53) and (54) with $\epsilon = 0$. As in the case of the Tucker program, average transmission coefficients obtained from the ABACUS II calculations using the non-local potential were used.

CHAPTER V

RESULTS AND CONCLUSIONS

A. Results

The experimental results and pertinent theoretical calculations are presented below. Elastic scattering angular distributions calculated using local and non-local potentials were essentially the same, and, therefore, only the angular distributions calculated with the non-local potential are shown. Surprisingly, however, the inelastic scattering cross sections calculated by ABACUS II using the non-local potential were significantly larger and their agreement with the data was, on the whole, significantly better than the same cross sections calculated using the local potentials. Therefore, in all calculations of inelastic scattering cross sections and mean square fluctuations of cross sections, the transmission coefficients resulting from the calculations with the non-local potential have been used.

Another surprising result of the calculations was that, although the elastic scattering angular distributions predicted by the non-local potential with reduced potential well depths differed significantly from those calculated using the original parameters of Perey and Buck, the inelastic scattering angular distributions calculated using the two sets of parameters were not significantly different.

The measured elastic scattering angular distributions for silicon are shown in figures 8 and 9. The data points have been corrected for multiple

scattering, beam attenuation, and geometrical effects using the Monte Carlo computer code. As described above, the input to the program is a smooth curve drawn through the measured data points. The points shown on the curve are these measured data points adjusted either up or down by the same factor by which the final "actual" angular distribution produced by the computer code differed at each observation angle from the "observed" angular distribution used as input.

There are four theoretical curves plotted along with each experimental angular distribution, all of which were calculated using the non-local optical potential.

The curves designated "Standard Wells - H.F. σ_{ce}" are each the sum of the shape elastic and compound elastic scattering angular distributions calculated by the computer code ABACUS II, where the parameters originally determined by Perey and Buck (Table III) have been used and where the compound elastic scattering cross section has been calculated using the standard Hauser-Feshbach formula, Eq. (20).

The curves designated "Standard Wells - Dresner σ_{ce}" are each calculated using the original well depths of Perey and Buck, but in this case, the compound elastic cross section has been corrected by the width fluctuation correction of Dresner, Eq. (32). Hereafter, we shall refer to compound cross sections calculated in this way as "Dresner" cross sections, and to those calculated using Eq. (20) as "Hauser-Feshbach" cross sections. The curves designated "Reduced Wells - H.F. σ_{ce}" and "Reduced Wells - Dresner σ_{ce}" result from the same calculations as above but with the well depths reduced by 10%.

Note that the agreement between theory and experiment generally improves with increasing bombarding energy. In particular at 4.9 and 5.8

Figure 8. Elastic Scattering Angular Distributions for Silicon at 2.45, 2.85, and 4.00 MeV

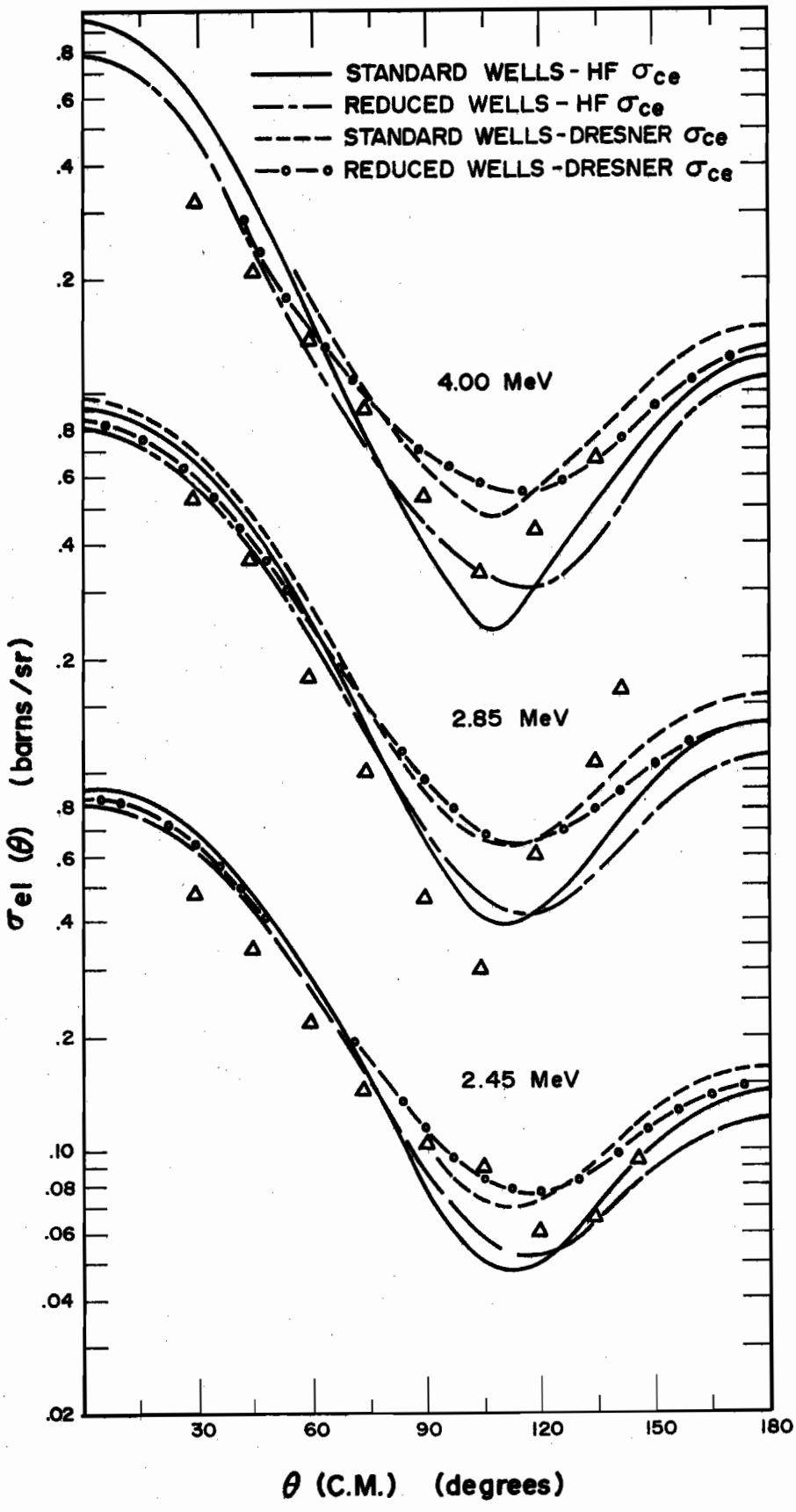
STANDARD WELLS - HF σ_{ce}
REDUCED WELLS - HF σ_{ce}
STANDARD WELLS - DRESNER σ_{ce}
REDUCED WELLS - DRESNER σ_{ce}
4.00 MeV
2.85 MeV
2.45 MeV
σ_{el} (θ) (barns/sr)
θ (C.M.) (degrees)
.8
.6
.4
.2
.10
.08
.06
.04
.02
30
60
90
120
150
180

Figure 9. Elastic Scattering Angular Distributions for Silicon at 4.9 and 5.8 MeV

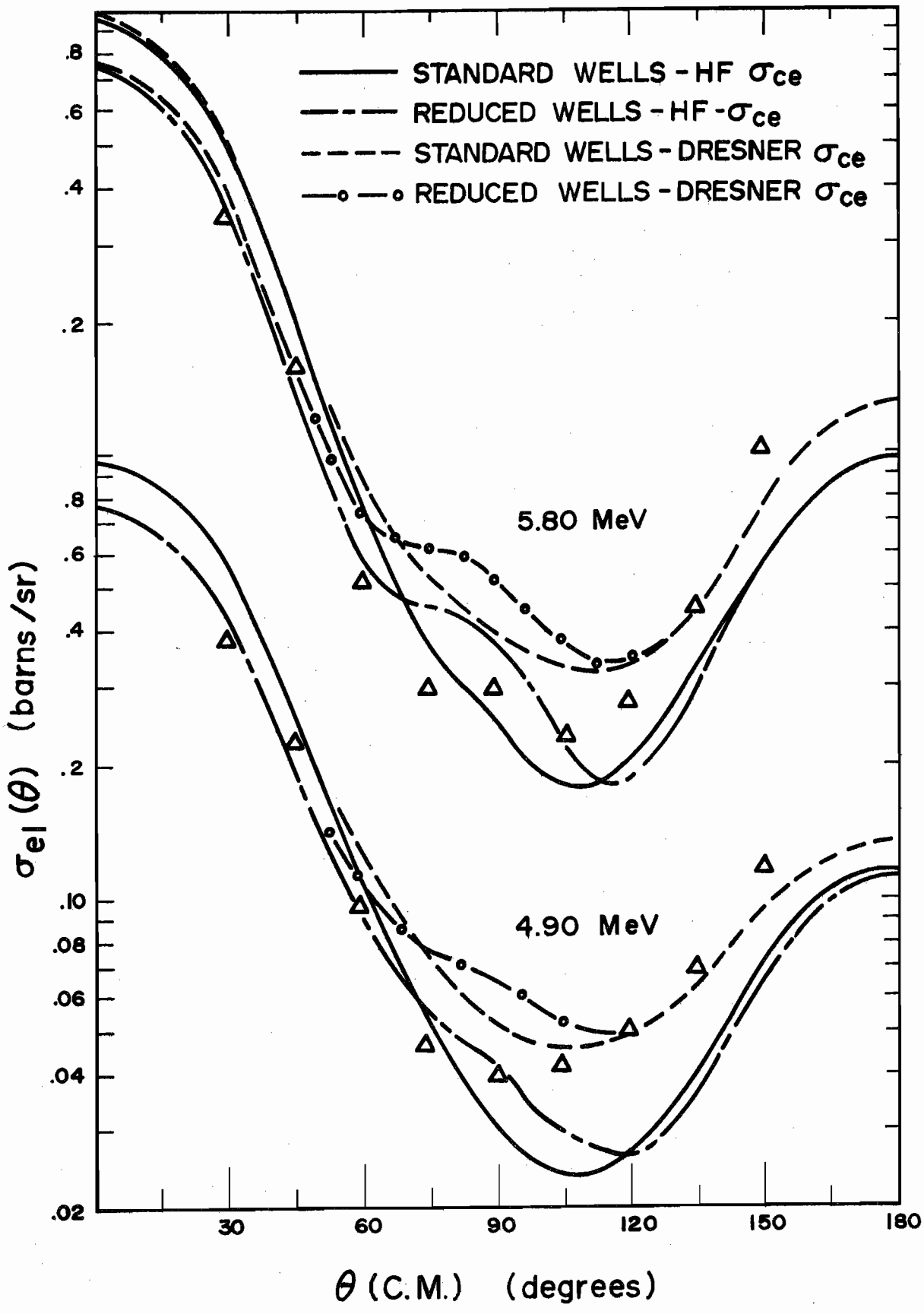
STANDARD WELLS - HF σ_{ce}
REDUCED WELLS - HF - σ_{ce}
STANDARD WELLS - DRESNER σ_{ce}
REDUCED WELLS - DRESNER σ_{ce}
5.80 MeV
4.90 MeV
$\sigma_{el}(\theta)$ (barns/sr)
θ (C.M.) (degrees)
.8
.6
.4
.2
.10
.08
.06
.04
.02
30
60
90
120
150
180

MeV, where fluctuation effects are expected to be smallest, the overall agreement between the data points and the theoretical curve obtained using the reduced well depths is fairly precise at forward angles. At the minimum and to a lesser extent at back angles, the cross section is dominated by the compound elastic scattering, and the fluctuation effects which are present in the compound reactions may be expected to preclude any precise agreement between theory and experiment even if the optical model description is valid for this nucleus. Nevertheless, there are two general features of the angular distributions at these angles that should be noted.

First, the minimum of the measured angular distributions is generally at an angle of 90° to 105° while the minimum in the theoretical curves calculated using the reduced well depths is between an angle of 105° and 120°. The agreement between the measured angular distributions and the theoretical curves calculated using the standard well depths is generally much better at the minimum. Therefore, by introducing the reduced well depths, the better agreement at the forward angles has been exchanged for a consistently poorer agreement at the minimum.

Second, despite this effect and except for the points at 75°, 90°, and 150°, the data points are at least bracketed by the curves calculated using the Hauser-Feshbach and Dresner compound elastic angular distributions.

Figures 10 and 11 show the measured 60° (lab angle) excitation curves for silicon and the corresponding theoretical predictions obtained using the Hauser-Feshbach and Dresner formulas. The differential cross sections at 60° scattering angle taken from the angular distribution measurements are also shown; the excitation curves were normalized to these points. The agreement between these two sets of data is remarkably good in light of the rapid variation with angle of the elastic scattering angular distribution and, as

Figure 10. Excitation Curves for Silicon Between 2.2 and 3.0 MeV

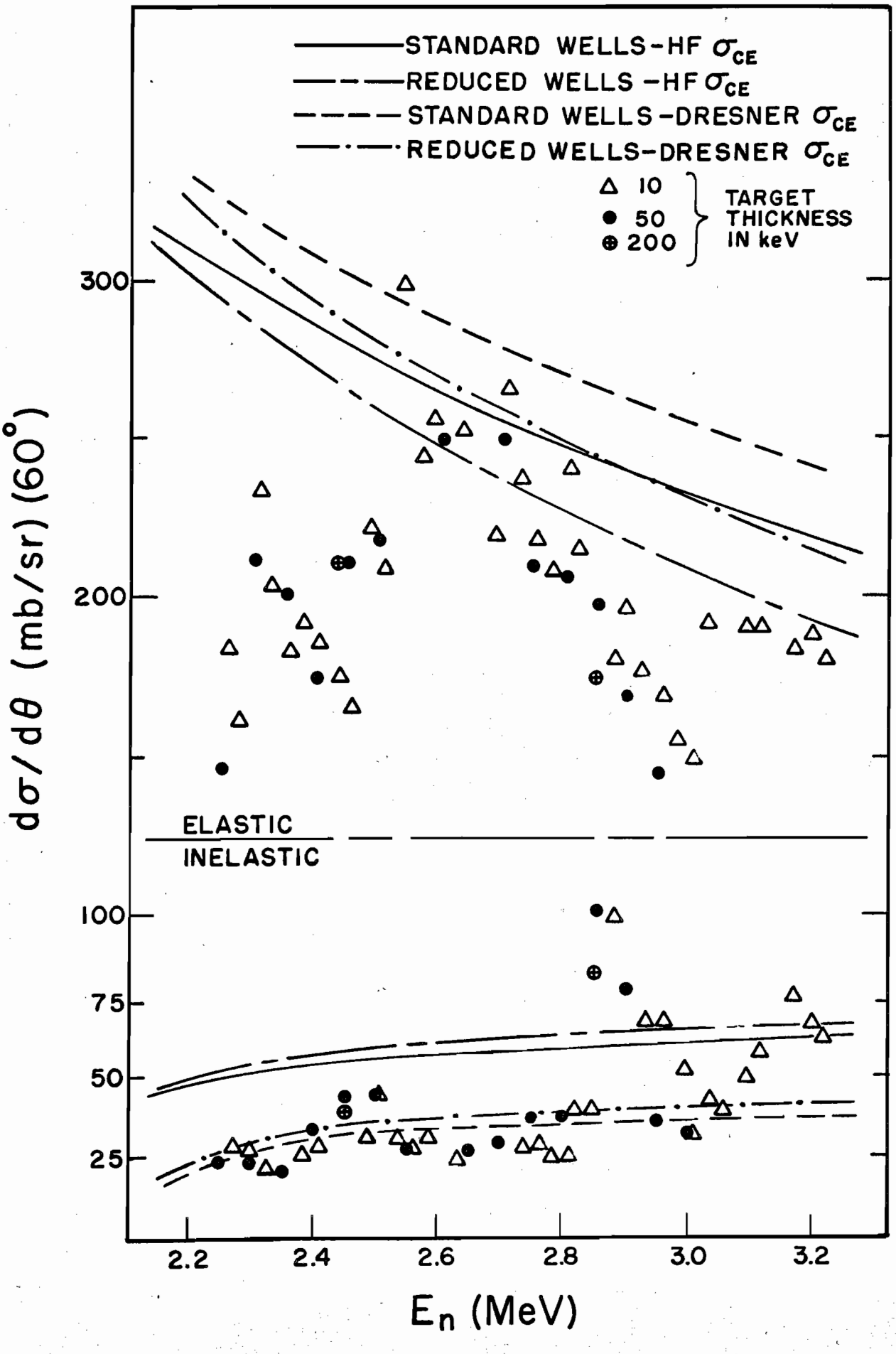
STANDARD WELLS-HF σ_{CE}
REDUCED WELLS-HF σ_{CE}
STANDARD WELLS-DRESNER σ_{CE}
REDUCED WELLS-DRESNER σ_{CE}
10
50
200
TARGET THICKNESS IN keV
ELASTIC
INELASTIC
300
200
100
75
50
25
2.2
2.4
2.6
2.8
3.0
3.2
$d\sigma/d\theta$ (mb/sr) (60°)
E_n (MeV)

Figure 11. Excitation Curves for Silicon and Sulfur Between 4 and 6 MeV

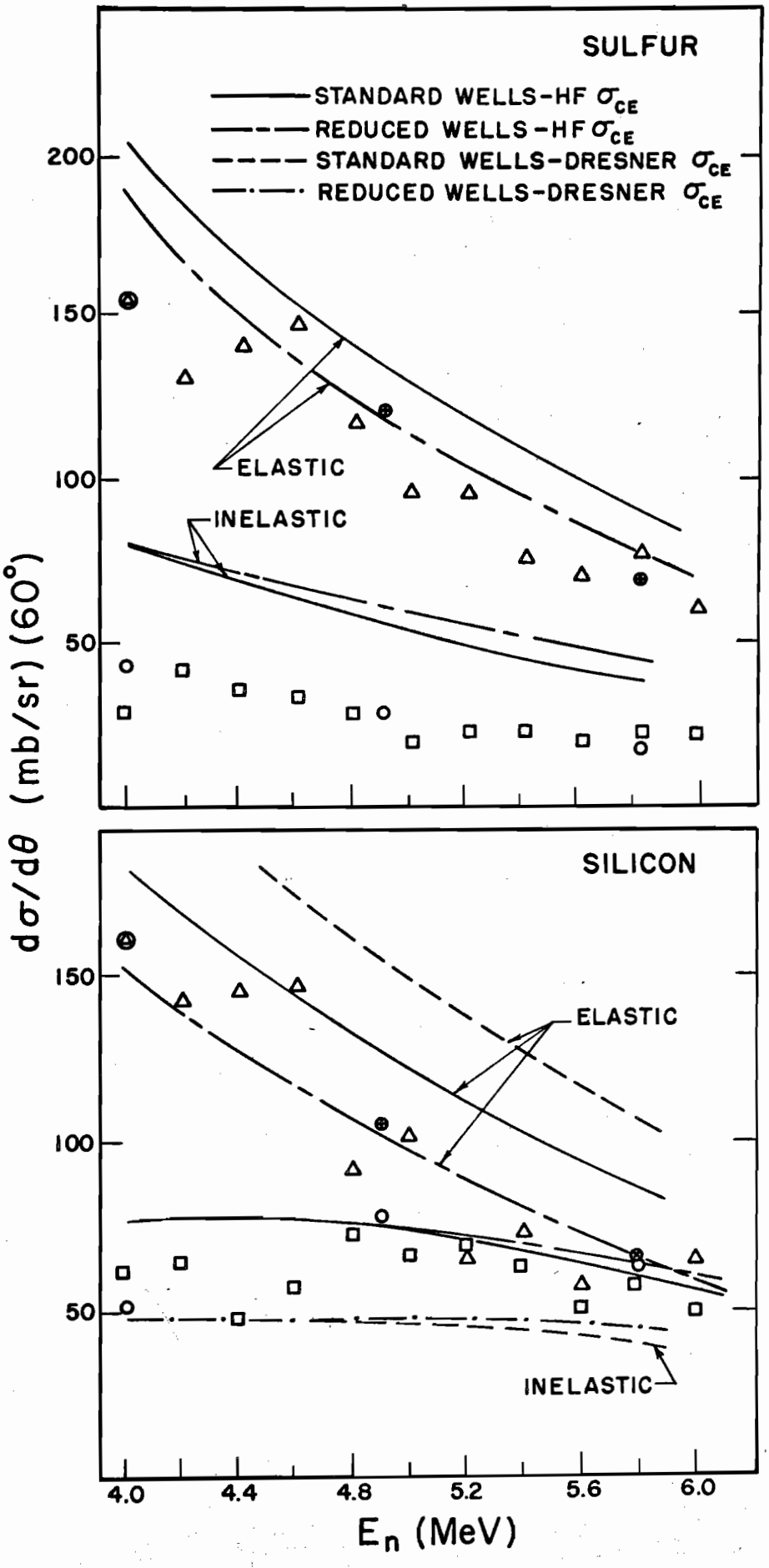
SULFUR
STANDARD WELLS-HF σ_{CE}
REDUCED WELLS-HF σ_{CE}
STANDARD WELLS-DRESNER σ_{CE}
REDUCED WELLS-DRESNER σ_{CE}
ELASTIC
INELASTIC
SILICON
ELASTIC
INELASTIC
200
150
100
50
150
100
50
4.0
4.4
4.8
5.2
5.6
6.0
$d\sigma/d\theta$ (mb/sr) (60°)
E_n (MeV)

noted previously, in light of the uncertainties in the corrections that were applied to the excitation curve data.

The inelastic scattering differential cross section obtained from the angular distribution at 2.85 MeV is much lower than the points measured in the excitation curves. This is expected because of the averaging effect of the very thick target used in measuring the angular distributions as opposed to the thin targets used in measuring the excitation curve (200 keV vs. 10 keV and 50 keV at threshold).

Both the elastic and inelastic curves show large fluctuations with energy, especially at the lower energies, so that precise agreement between theory and experiment cannot be expected. Note especially that the two lowest energies at which angular distributions were taken correspond to peaks of the fluctuations in the inelastic excitation curve.

Aside from fluctuation effects, the rapid variation with angle of the elastic scattering angular distribution makes a comparison between theory and experiment rather meaningless. Nevertheless, it is worth noting that at the higher bombarding energies, the theoretical cross sections all decrease with energy at about the same rate as the excitation curves.

Due to the near isotropy of the inelastic scattering angular distributions, it is quite reasonable to make a direct comparison between theory and experiment at a single angle. At all energies, after averaging over the fluctuations, the experimental curves generally fall between the Hauser-Feshbach and Dresner predictions as was the case at the minimum in the elastic scattering angular distributions where compound elastic scattering dominated the cross section.

At the lowest energies, up to the large fluctuation at around 2.85 MeV, the Dresner curve clearly matches the data much better than the Hauser-

Feshbach curve. Above this energy, the average falls midway between the two theoretical curves.

We have noted previously a number of possible explanations for this behavior:

The presence of a small direct reaction component may increase the average value of the cross section above the Dresner prediction. However, the inelastic scattering angular distributions fail to show the assymetry that is associated with direct reactions. This is true for both silicon and sulfur at all bombarding energies. The shapes of the angular distributions are, on the average, symmetric about 90°, which is consistent with the assumption that the scattering takes place by formation and decay of the compound nucleus.

Secondly, if the assumption that $\langle \Gamma^{J\pi} \rangle \gg D_{J\pi}$ is not fulfilled, the average cross sections may be increased above the values predicted by the Dresner formula.

We have noted previously that Moldauer (1963) has calculated a number of inelastic scattering cross sections with the assumption that $\langle \Gamma^{J\pi} \rangle \approx D_{J\pi}$ in which case the assumed distribution of level spacings affects the results, and that the magnitudes of the resulting cross sections generally fall between the magnitudes calculated using the Hauser-Feshbach and Dresner formulas. These calculations were not exact since they contained parameters whose values had to be crudely estimated. They nevertheless represent a "first guess" at the kind of correction to be made to the Dresner formula if the requirement that $\langle \Gamma^{J\pi} \rangle \gg D_{J\pi}$ does not hold. This suggests that this requirement may not be fulfilled in the case of silicon at these bombarding energies.

These two are, of course, not the only possible explanations for the disagreement between theory and experiment. The possibility of direct reactions

is worthy of mention simply because there is evidence from the shapes of the angular distributions that direct reactions are not taking place. The second explanation is mentioned because it does not actually involve the breakdown of any of the assumptions of statistical model theory, but is simply the result of applying the statistical assumptions to a special experimental situation; namely, to the situation where $\langle \Gamma^{J\pi} \rangle \approx D_{J\pi}$ which is quite possibly true for the compound system in this case.

The fluctuations in the excitation curves are presumably of the type described by Ericson. That is, they result from the interferences between the amplitudes of the many resonances which simultaneously dominate the cross section. As pointed out by Moldauer (1964), the fluctuations will be somewhat larger than those predicted by Ericson (Eq. 55) in the case where $\langle \Gamma^{J\pi} \rangle \approx D_{J\pi}$. Since we can expect only order-of-magnitude agreement between calculated mean square fluctuations and those measured experimentally over a finite energy interval, we have made these comparisons, using Ericson's formulas and ignoring the possibility of their being slightly incorrect in the case of silicon if the assumption that $\langle \Gamma^{J\pi} \rangle >> D_{J\pi}$ is not fulfilled.

Table IV shows some typical values of the average square fluctuation of the total cross section and inelastic scattering cross section. All values are in $(\text{barns})^2$. The energy intervals over which the averages were measured are also shown. These are compared with the corresponding average square fluctuations calculated using the formulas of Ericson (equations (53) and (54)). Transmission coefficients obtained from the optical model calculations with reduced potential well depths were used in these calculations. The results are essentially the same when transmission coefficients resulting from calculations with the standard well depths are used.

Table IV. Mean Square Fluctuations in Total and Inelastic Cross Sections

	Silicon		Sulfur	
E_n (MeV)	$\langle(\delta\sigma_T(E))^2\rangle$ (barns)	$\langle(\delta\sigma_{nn'}(E))^2\rangle$ (barns)	$\langle(\delta\sigma_T(E))^2\rangle$ (barns)	$\langle(\delta\sigma_{nn'}(E))^2\rangle$ (barns)
2.45	.57	.07	.94	.02
2.85	.42	.08	.53	.06
2.3-3.0	.14	---	.05	---
2.2-3.2	---	.06	---	---
4.00	.26	.06	.30	.06
4.90	.21	.04	.17	.02
4.0-5.0	.11	---	.12	.01
4.0-5.8	---	.01	---	---
5.80	.14	.02	.11	.01

Where single bombarding energy is indicated in first column, values in other columns are calculated using Ericson's formulas. Where range of bombarding energies are indicated in first column, values in other columns are taken from experimental data.

The lower energy total cross section fluctuation measurements were taken from the curves in BNL 325. At the higher energies, the results of Tsukada and Tanaka (1963) were used. The fluctuations in the inelastic cross sections were estimated by measuring the fluctuations in the 60° excitation curves measured in this experiment.

The measured and calculated averages for silicon generally agree to at least within a factor of three or four which is reasonable agreement for averages over a few fluctuations.

The large size of the fluctuation at 2.85 MeV in the inelastic scattering cross section makes it an interesting candidate for a "doorway state" resonance. However, if it is such a resonance, it should also appear in the compound elastic scattering cross section at the same incident neutron energy. At 60° scattering angle, the compound elastic component of the total elastic scattering should be large enough for the resonance to be seen. However, there is no evidence of its existence in the elastic excitation curve. There is an observable fluctuation in the total cross section at this energy, but this can be accounted for by assuming that it is due entirely to the fluctuation in the inelastic cross section. Therefore, this fluctuation is presumed not to be a "doorway state" resonance.

The inelastic scattering angular distributions for silicon are shown in Fig. 12. The theoretical curves shown are the results of the calculations using the Hauser-Feshbach formula. These cross sections were always reduced when Dresner's width fluctuation correction was applied. The reductions are shown by arrows whose tips are at the Dresner cross section values. As mentioned above, the Dresner angular distributions were not calculated but are assumed to have the same nearly isotropic shape as the Hauser-Feshbach curves.

Figure 12. Inelastic Scattering Angular Distributions for Silicon

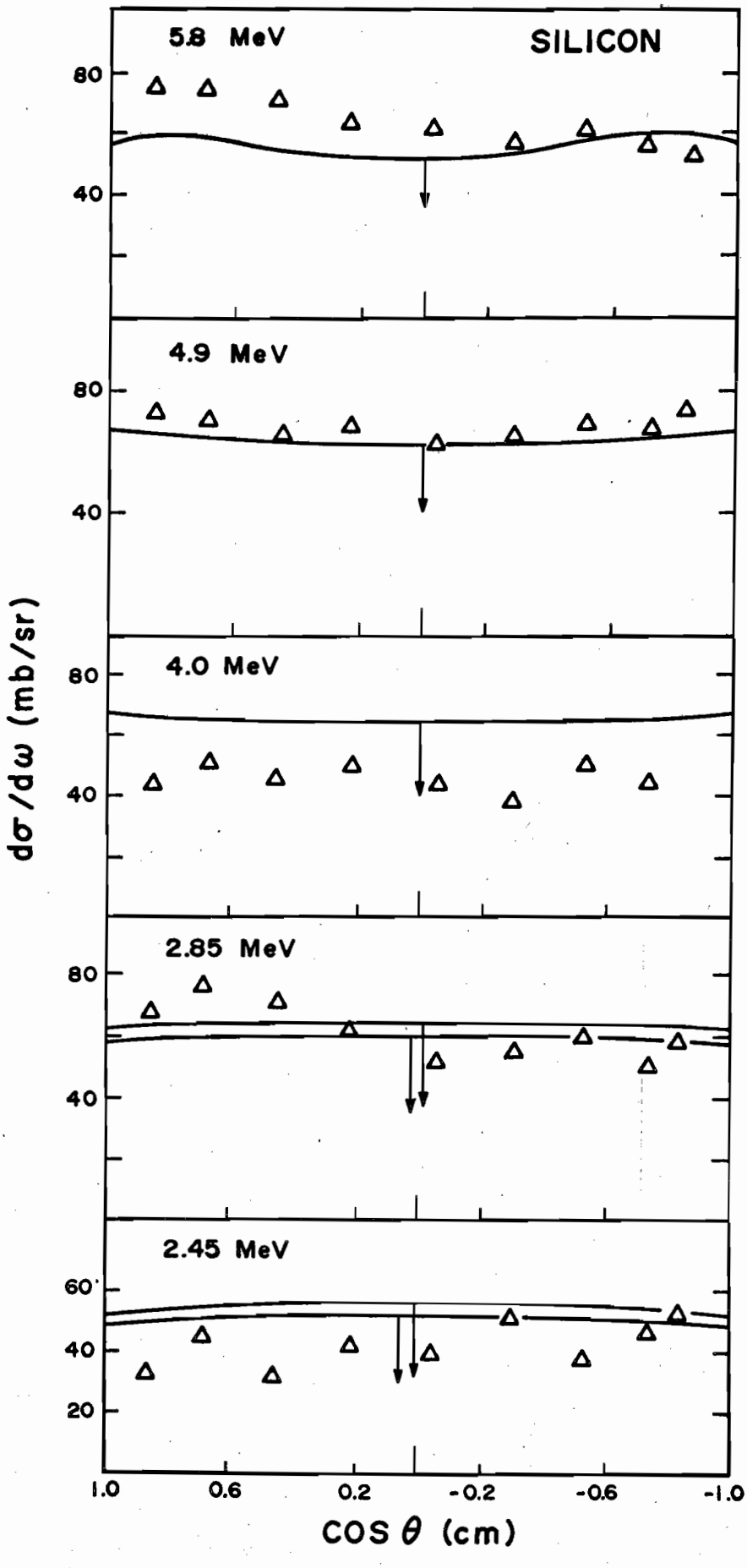
5.8 MeV
SILICON
80
40
4.9 MeV
80
40
4.0 MeV
80
40
2.85 MeV
80
40
2.45 MeV
60
40
20
dσ/dω (mb/sr)
1.0
0.6
0.2
-0.2
-0.6
-1.0
COS θ (cm)

Lind and Day (1961) have measured the excitation of the first level in silicon at a laboratory angle of about 95° up to 3 MeV incident neutron energy. The fluctuations in their excitation curve are similar to those observed in our 60° excitation curve. At 60° the P_2 term in the Legendre polynomial expansion of the angular distribution is almost zero and the P_0 term dominates. Therefore, we should expect the fluctuations in our excitation curves to be about the same as those in the integrated cross section which depends only on the fluctuations in the P_0 term. The fluctuations in the excitation curves and integrated cross sections are larger than the fluctuations in the angular distributions. In general, the reverse should be true since the integrated cross sections and their fluctuations depend only on the P_0 Legendre polynomial term, whereas the angular distributions and their fluctuations depend on the higher order polynomials. In this case, the angular distributions are so isotropic that they and their fluctuations are apparently dominated by the P_0 term and the fluctuations in the higher order polynomials have little effect on the angular distribution. Also, at the two lowest bombarding energies, the energy spread in the incident beam due to target thickness was much larger for the angular distribution measurements than for the excitation curve measurements which tends to dampen the fluctuations in the angular distribution compared to the excitation curve.

The elastic scattering angular distributions for sulfur are shown in figures 13 and 14. The same corrections have been made to the data points as were made for the silicon angular distributions. The two theoretical curves shown are the sum of the shape elastic and compound elastic cross sections. The Hauser-Feshbach formula was used to calculate the compound elastic cross section. This calculation is incorrect because only neutron

Figure 13. Elastic Scattering Angular Distributions for Sulfur at 2.45, 2.85, and 4.00 MeV

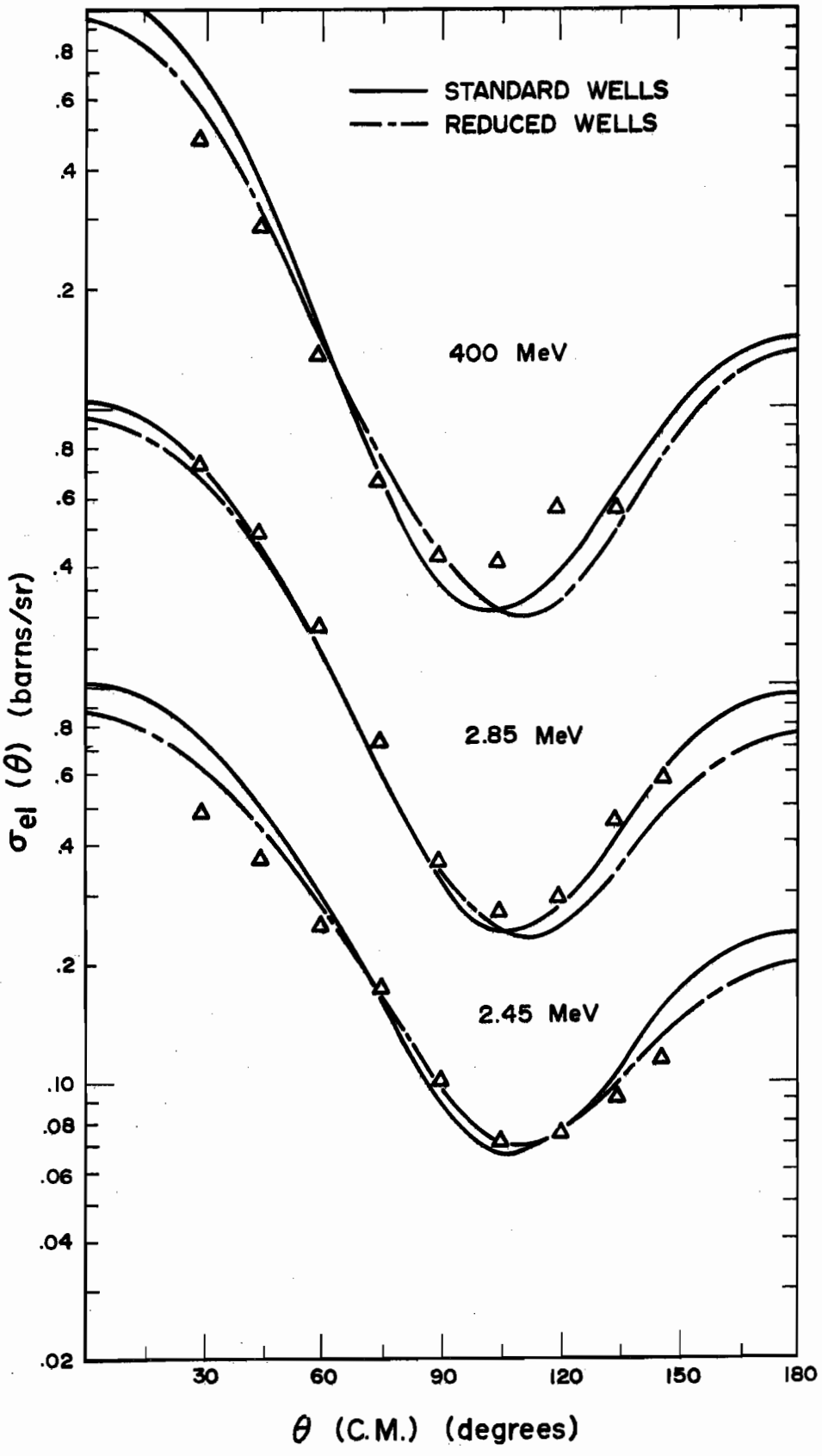
STANDARD WELLS
REDUCED WELLS
400 MeV
2.85 MeV
2.45 MeV
σ_{el} (θ) (barns/sr)
θ (C.M.) (degrees)
.8
.6
.4
.2
.10
.08
.06
.04
.02
30
60
90
120
150
180

Figure 14. Elastic Scattering Angular Distributions for Sulfur at 4.9 and 5.8 MeV

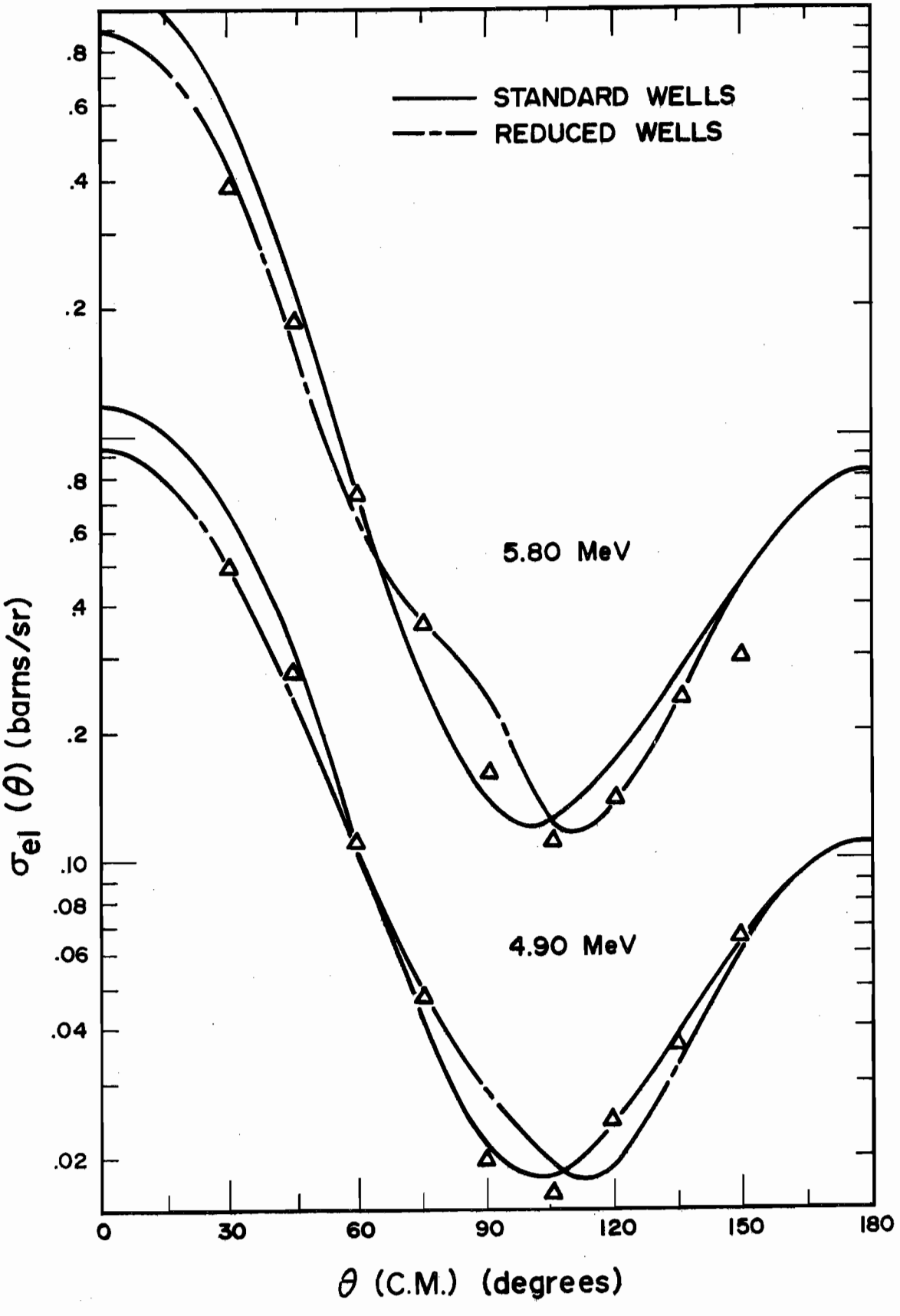
STANDARD WELLS
REDUCED WELLS
5.80 MeV
4.90 MeV
σ_{el} (θ) (barns/sr)
θ (C.M.) (degrees)
.8
.6
.4
.2
.10
.08
.06
.04
.02
0
30
60
90
120
150
180

emission is included in the branching ratio of the formula which results in a prediction that is too large. Since the (n,p) and (n,α) cross sections are roughly equal to the compound scattering cross section at all energies, our calculated values are, to a first approximation, about double what they would be if all competing reactions were taken into account. However, the Dresner correction invariably increases the compound elastic prediction, sometimes by as much as a factor of two. Since there are so many competing decay channels, it probably would not increase it by a factor of two in this case, even to a first approximation. Therefore, the compound elastic scattering cross sections calculated are probably only slight overestimates of the elastic scattering angular distribution that would be predicted using the Dresner formula to calculate the compound elastic scattering with all competing decay channels taken into account in the formula. Note that, as in the case of silicon, the curves predicted using the reduced well depths generally match the data better at the forward angles where shape elastic scattering dominates the cross section.

Due to the fact that the compound elastic scattering has not been calculated correctly, the agreement or lack of agreement around the minimum (75° - 135°) is not significant.

The sulfur excitation curve is shown in Fig. 11. Note that the fluctuations in the elastic and inelastic curves are smaller than those in the silicon curves by about a factor of two. This is presumably due to the damping effect of the many open decay channels for sulfur. A comparison of the measured and calculated quantities for sulfur in Table II is misleading since at the higher energies the calculated and measured quantities agree well, whereas at the lower energies the calculated and measured mean square fluctuations in the total cross section differ by at least a factor of ten.

The reason for the large discrepancy at the lower energy is due to the fact that the only decay channels included in the calculations were elastic and inelastic neutron scattering whereas there is actually a large (n,p) cross section. At the higher energies the discrepancy between measured and calculated mean square fluctuations is not nearly as great since, although the competing (n,p) and (n,α) cross sections are not taken into account in the calculations, they are a less significant part of the total cross section than at the lower energies.

The Hauser-Feshbach inelastic scattering cross sections shown are generally more than twice the measured cross sections. This is also presumably due to the many decay channels that are not accounted for in the calculations. As in the case of the compound elastic cross section, the many competing reactions would probably decrease the calculated cross section by about a factor of two if they could be properly taken into account. The Dresner correction would not be expected to decrease this much further because of the many open decay channels. The net result would be to give fair agreement between theory and experiment.

The measured inelastic cross sections for sulfur are shown in Fig. 15. No theoretical comparisons have been made in this case since the theoretical calculations cannot be done correctly. Note that the fluctuations in the angular distributions are apparently larger than in the excitation curve and are larger than the fluctuations in the silicon inelastic scattering angular distributions at these energies. If we assume that the fluctuations in the excitation curve are roughly the same as those in the integrated cross section, then the fact that the fluctuations in the angular distribution are slightly larger than in the excitation curve is in agreement with the predictions of Ericson.

Figure 15. Inelastic Scattering Angular Distributions for Sulfur

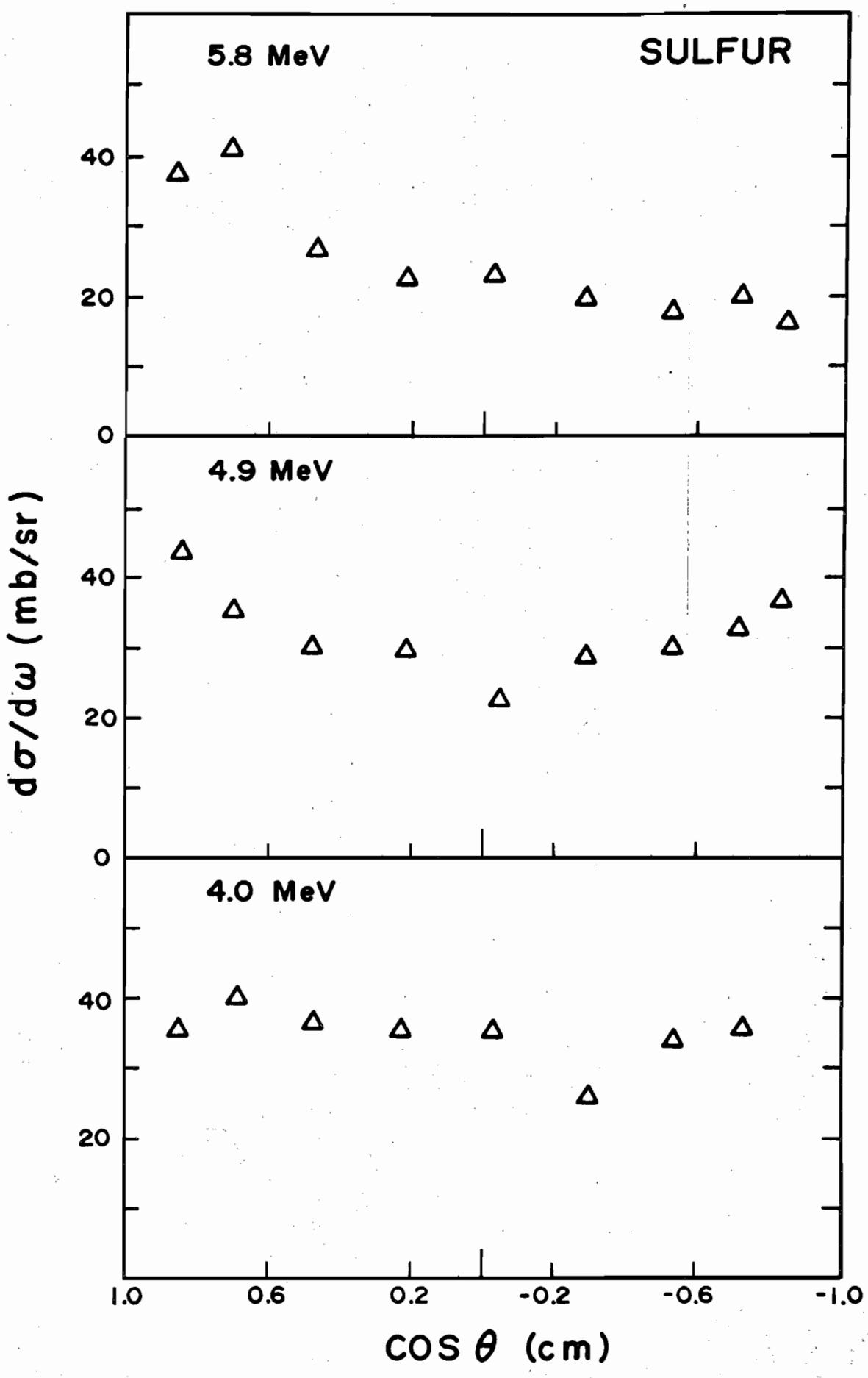
5.8 MeV
SULFUR
4.9 MeV
4.0 MeV
dσ/dω (mb/sr)
40
20
0
1.0
0.6
0.2
-0.2
-0.6
-1.0
COS θ (cm)

The results are summarized in Table I. The first column lists the total cross sections obtained by other workers. The next two columns list the elastic and inelastic scattering cross sections measured in this experiment and the fourth and fifth columns list the available (n,p) and (n,α) cross sections from other experiments. At all energies where cross sections are known for all competing reactions and are added to the scattering cross sections measured in this experiment, the sum is found to agree with the total cross sections in column I to within about 5%. In order to make a comparison at the higher energies in the case of silicon, an estimate had to be made of the inelastic cross section for excitation of the second excited state which could not be measured. In the case of sulfur, the inelastic cross sections at the two lower energies had to be estimated as well as the (n,p) and (n,α) cross sections which have not been measured. Using reasonable estimates of these cross sections, good agreement was obtained between the sum of the partial cross sections and the independently measured total cross sections.

In the last two columns are listed the inelastic scattering cross sections calculated using the Hauser-Feshbach and Dresner formulas with the transmission coefficients resulting from the calculations with the non-local potential using the reduced well depths. The inelastic cross sections calculated using the standard well depths differed from these by at most about 5% so they have been omitted. In the case of silicon, although the measured cross sections listed in the table agree in general much better with the Hauser-Feshbach than with the Dresner predictions, the excitation curves give a much better picture of the overall behavior of the cross sections. At the lower energies, the angular distributions were deliberately taken on the peaks of fluctuations and at the higher energies all except the 4 MeV

angular distributions happened to be at the peak of a fluctuation as can be seen on the excitation curves.

B. Conclusions

The results of this experiment may be summarized as follows: The nonlocal potential of ~~Prey~~ Perey and Buck with the potential well depths reduced slightly from their original values describes the shape elastic component of neutron scattering from silicon and surfur for high incident neutron energies where fluctuation effects are small.

The inelastic scattering cross sections for silicon show large flucuations, and the average inelastic scattering cross section is generally smaller than the predictions of the Hauser-Feshbach formula and larger than the predictions of the Hauser-Feshbach formula modified by the width fluctuation correction of Lane, Lynn, and Dresner where a Porter-Thomas distribution of partial widths is assumed and transmission coefficients from the non-local optical potential calculations are used in the formulas.

The excess of the cross sections over the predicted values is probably not due to direct reactions since the angular distributions do not show the strong forward peaking characteristic of direct reactions but are, on the average, symmetric about 90°. Rather, the magnitude of the cross sections are such that the discrepancy may reasonably be ascribed to the breakdown of the assumption that $\langle \Gamma^{J\pi} \rangle \gg D_{J\pi}$ for the compound system.

The fluctuations in the cross sections are apparently of the type described by Ericson and his formulas are useful in obtaining order of magnitude estimates of the mean square fluctuations in the cross sections for these elements.

In accordance with Ericson's predictions, the fluctuations in the angular distributions for sulfur are larger than those in the integrated cross sections. In the case of silicon, however, the reverse is true.

Due to the large (n,p) and (n,α) cross sections for sulfur, which cannot be taken into account in the calculations of the cross sections for inelastic neutron scattering, no conclusions can be drawn about the agreement or lack of agreement of the measured cross sections with theory except that if the appropriate proton and alpha particle emission probabilities could be determined for use in the Hauser-Feshbach formula, the resulting calculated cross sections would match the measured cross sections fairly well.

APPENDIX

APPENDIX

MANIAC is a Fortran computer code which calculates the effects on an experimentally measured neutron scattering angular distribution due to the finite size of the scatterer. These effects include attenuation of the incoming neutron beam, multiple scattering of the neutrons in the scatterer, and the finite range of actual scattering angles at which neutrons are scattered to each detector position.

The program simulates the scattering experiment by following the paths of many neutrons from a source, through a scatterer, to a group of detectors placed in a ring around the scatterer. The paths of the neutrons are chosen randomly, and each detected neutron is weighted according to the probability that it would reach the detector.

Running totals of these weighted neutrons are kept for each detector. The program normalizes these sums to yield an "observed" angular distribution. Thus, if an angular distribution free of the effects of multiple scattering, beam attenuation, and geometrical effects is used as input to the program, the final output will be an angular distribution which closely approximates the actual measured angular distribution. An iterative procedure may be used to obtain the angular distribution that would be measured in the absence of these effects.

The program simulates the experimental arrangement as follows. A cylindrical scattering sample with the same dimensions as the one actually

used in the experiment is surrounded by a band of detectors. As many detectors can be used as desired up to 37. These hypothetical detectors have the same height as the detector actually used in the experiment and are the same distance from the scatterer. It is assumed that the horizontal dimension of each detector is so small that it may be neglected. Therefore, the detectors are simply vertical lines which the program forces the neutron trajectories to intercept. Each neutron "history" begins when the neutron emerges from a point source which is the same distance from the scattering sample as in the actual experiment. The angular distribution of the source reaction is used to weight each neutron according to the probability that it would actually emerge in that direction. The scattering angle for the first collision is chosen randomly, and the elastic scattering angular distribution is used to weight the neutron according to the probability that it would actually scatter through this angle. (Note that this angle is not necessarily one of the angles at which a detector is placed with respect to the incident beam direction; the scattered neutron may or may not intercept a detector.)

The program then calculates the probability that the weighted neutron would not escape from the sample without having a second collision. This probability represents the fraction of the original neutron which scatters a second time. In fact, this second scattered neutron fraction is divided into many smaller fractions, one for each of the detectors in the detection band, and each is then forced to scatter into one of the detectors. These second scattered neutron fractions are weighted by the probability that they would scatter in the direction of the detector. In this case, it is not strictly a weight given the neutron fraction. Rather, the weighted value of the neutron fraction is multiplied by the differential cross section for scattering at this angle. When the total number of detected neutrons is normalized, the result is an angular distribution in units of mb/sr.

The second scattered neutron fractions are not weighted by the probability that they will escape without having further collisions. Instead, they are allowed to escape completely and no further collisions are considered. Thus, the program overestimates the amount of double scattering while ignoring the possibility that any number of subsequent scatterings can actually occur or that the neutrons can be lost (due to inelastic scattering) before they escape. This does not introduce any significant error, however, since the angular distribution of the doubly scattered neutrons is, in all cases, very nearly isotropic, and the angular distribution of neutrons scattered more times could be expected to be even more isotropic. Except for the neutrons lost due to subsequent inelastic scattering, the total number of neutrons detected will be the same as if subsequent scattering were considered, since all second scattered neutrons due to further elastic scatters would eventually reach a detector. Thus, a small error is introduced by ignoring the possibility of subsequent inelastic scattering, and there is a slight error in the shape of the multiple scattering angular distribution due to the fact that only double scattering is considered.

In order to obtain the correct angular distribution for double scattering, it is necessary to choose the first scattering angle randomly. Unfortunately, only a small fraction of these singly scattered neutrons intercept one of the detectors. In order to increase the speed of the program, these neutrons are not utilized in counting the number of singly scattered neutrons. Instead, after the program has recorded the doubly scattered neutrons, it returns to the point in the scatterer at which the first scattering occurred. One neutron is scattered into each detector from this point. Each one is allowed to escape completely but is weighted according to the probability that it would scatter in the direction of the detector. As in the

case of the previously calculated double scattering, the weighted neutrons are multiplied by the differential cross section for elastic scattering at this angle so that when the weighted sum is normalized an observed angular distribution in units of millibarns per steradian is obtained.

The normalization for both single and double scattering consists of dividing the weighted neutron totals by the totals of all the weights given each neutron except for the following:

1) The differential cross section by which each weighted neutron is multiplied when it is scattered. (The differential cross section for the second scatter in the case of double scattered neutrons)
2) The probability that the original neutron would emerge from the source at the angle chosen for it (normalized to unity at 0°).

The result is the angular distribution that would be measured if the neutron flux incident on the sample were assumed to be colinear and uniform, and equal to the flux incident on the sample at 0°. Thus, the ratio of the "observed" and "theoretical" elastic cross sections is a measure of the attenuation of a fictitious uniform incident neutron beam.

The program is principally designed to make corrections to elastic scattering angular distributions. However, it may also be used to simultaneously make corrections to an inelastic scattering angular distribution where the residual nucleus is left in one of its discrete excited states after the scattering. In this case, the program assumes that the inelastic scattering angular distribution is isotropic. Only the value of the angle integrated angular distribution is read in. The program then makes essentially the same calculations for the inelastic angular distribution as for the elastic except that no values of $\frac{d\sigma}{d\Omega}$ enter the calculations, and the program calculates the contribution due to neutrons that scatter inelastically after first

being elastically scattered, and the contribution due to neutrons which scatter elastically after first being scattered inelastically.

In addition to approximating all multiple scattering by double scattering, the program makes several other approximations. Some of these may cause serious error if the detector is very close to the scatterer. The program also does not take into account the variation with angle of the scattered neutron energy. This may cause serious errors in the case of scattering from light elements where the program will count neutrons which are scattered twice through large angles after which they might lose so much energy to the recoiling nuclei that they would not actually be detected by an energy sensitive detector.

LIST OF REFERENCES

LIST OF REFERENCES

E. H. Auerbach, private communication (1963).

W. Hauser and H. Feshbach, Phys. Rev. 87, 366 (1952).

N. Bohr, Nature 137, 344 (1936).

J. M. Blatt and V. F. Weisskopf, Theoretical Nuclear Physics, (John Wiley and Sons, New York, 1952).

H. Feshbach, Ann. Phys. (N. Y.) 19, 287 (1962).

H. Feshbach and V. Weisskopf, Phys. Rev. 76, 1550 (1949).

H. Barschall, Phys. Rev. 86, 431 (1952).

H. Feshbach, C. E. Porter, and V. F. Weisskopf, Phys. Rev. 96, 448 (1954).

F. Perey and B. Buck, Nucl. Phys. 32, 353 (1962).

F. L. Friedman and V. F. Weisskopf, Neils Bohr and the Development of Physics (Pergamon Press, New York, 1955).

R. D. Woods and D. S. Saxon, Phys. Rev. 95, 557 (1954).

J. M. Blatt and L. C. Biedenharn, Rev. Mod. Phys. 24, 258 (1952).

C. E. Porter and R. G. Thomas, Phys. Rev. 104, 483 (1956).

E. P. Wigner, Proc. Conf. on Neutron Phys. by Time-of-Flight, Gatlinburg, Tennessee, (1956).

A. M. Lane and J. E. Lynn, Proc. Phys. Soc. (London) A70, 557 (1957).

L. Dresner, Columbia University Report CU - 175, 71 (1957).

P. A. Moldauer, Rev. Mod. Phys. 36, 1079 (1964).

T. Ericson, Ann. Phys. (N. Y.) 23, 390 (1963).

S. Blumberg and C. E Porter, Phys. Rev. 110, 7867 (1958).

P. A. Moldauer, "Nuclear Cross Section Fluctuations" (unpublished) 1964.

H. W. Lewis, P. R. Bevington, W. W. Rolland, R. L. Rummel, and R. M. Wilenzick, Rev. Sci. Instr. 30, 923 (1959).

C. J. Kapadia, unpublished Masters thesis, Duke University (1963).

S. G. Buccino, unpublished Ph.D. dissertation, Duke University (1963).

C. E. Hollandsworth, unpublished Ph.D. dissertation, Duke University (1963).

R. M. Wilenzick, unpublished Ph.D. dissertation, Duke University (1962).

P. R. Bevington, unpublished Ph.D. dissertation, Duke University (1960).

W. W. Rolland, unpublished Ph.D. dissertation, Duke University (1963).

P. B. Parks, private communication (1963).

C. E. Hollandsworth, S. G. Buccino, and P. R. Bevington, Nuclear Instr. and Methods 28, 353 (1964).

W. Weber, C. W. Johnstone, and L. Cranberg, Rev. Sci. Instr. 27, 166 (1956).

W. D. Brooks, Nuclear Instr. and Methods 4, 151 (1959).

W. Daehnick and R. Sherr, Rev. Sci. Instr. 32, 666 (1961).

S. G. Buccino, C. E. Hollandsworth, and P. R. Bevington, Nucl. Phys. 53, 375 (1964).

D. B. Thomson, L. Cranberg, and J. S. Levin, Phys. Rev. 125, 2049 (1962).

J. H. Towle and W. B. Gilboy, Nucl. Phys. 32, 610 (1962).(a)

J. H. Towle and W. B. Gilboy, Nucl. Phys. 39, 300 (1962).(b)

P. R. Bevington, S. G. Buccino, and C. E. Hollandsworth, to be published.

Neutron Cross Sections, II ed., B. N. L. 325 (1958).

J. L. Fowler and J. E. Brolley, Rev. Mod. Phys. 28, 2 (1956).

F. E. Bjorklund and S. Fernbach, University of California Radiation Lab. Report UCRL 5028 (1958).

R. Hofstadter, Rev. Mod. Phys. 28, 214 (1956).

A. B. Tucker, J. T. Wells, and W. E. Meyerhoff, to be published.

K. Tsukada and O. Tanaka, J. Phys. Soc. Japan, 18, 610 (1963).

D. A. Lind and R. B. Day, Ann. Phys. (N. Y.) 12, 485 (1961).

BIOGRAPHY

Gus A. Petitt

Born: April 7, 1937, Birmingham, Alabama

Education:

B. S. Massachusetts Institute of Technology 1960

Professional Society:

Southeastern Section, American Physical Society

Positions:

Teaching Assistant, Duke University	1960 - 1961
Research Assistant, Duke University	1961 - 1964
Technical Staff, Northrop Space Laboratories	1964 - present

Abstracts:

Neutron Yields from the $Li^7(p,n')Be^7$ Reaction Near Threshold (with Buccino, Hollandsworth, and Bevington), Bull. Am. Phys. Soc. 8, 320 (1963).

Scattering of Fast Neutrons by Silicon and Sulfur (with Buccino, Hollandsworth, and Bevington) Bull. Am. Phys. Soc. 9, 78 (1964).